cmgh
CELLULAR AND MOLECULAR GASTROENTEROLOGY AND HEPATOLOGY

ORIGINAL RESEARCH

RBPJ Deficiency Sensitizes Pancreatic Acinar Cells to KRAS-Mediated Pancreatic Intraepithelial Neoplasia Initiation

Leiling Pan,[1,*] Medhanie A. Mulaw,[2,*] Johann Gout,[1] Min Guo,[1] Hina Zarrin,[1] Peggy Schwarz,[1] Bernd Baumann,[3] Thomas Seufferlein,[1] Martin Wagner,[1] and Franz Oswald[1]

[1]*Department of Internal Medicine I, Center for Internal Medicine, University Medical Center Ulm, Ulm, Germany;* [2]*Unit for Single-cell Genomics, Medical Faculty, Ulm University, Ulm, Germany; and* [3]*Institute of Physiological Chemistry, Ulm University, Ulm, Germany*

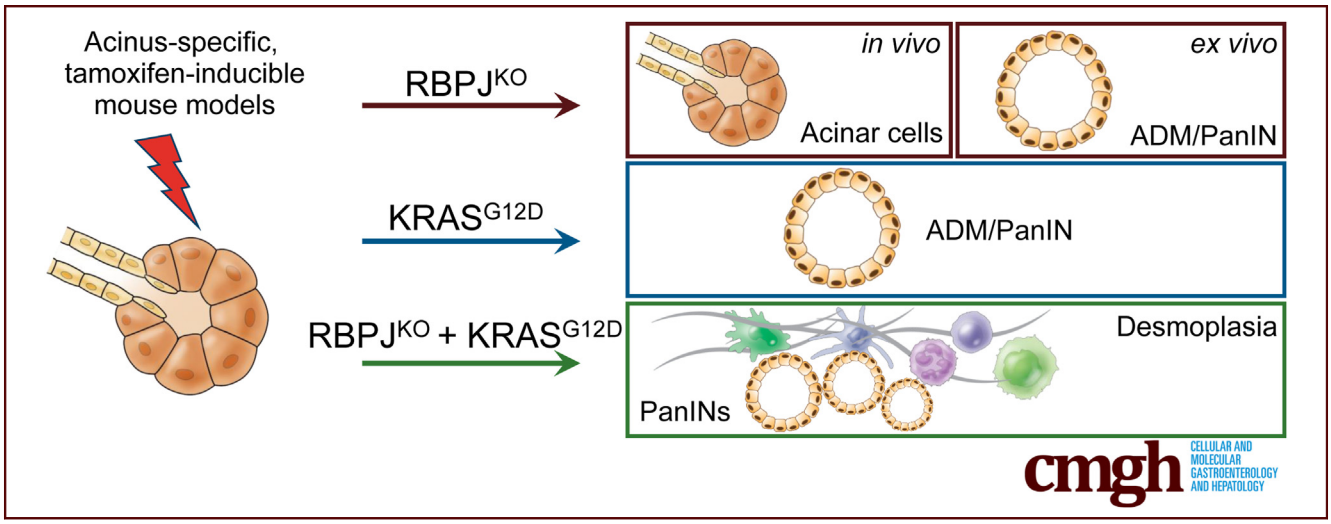

SUMMARY

RBPJ, a central component in Notch signaling, is dispensable for the maintenance of adult acinar cells. However, its frequent down-regulation in PDAC patients together with the results from our study suggest a critical tumor-suppressor-function of RBPJ in KRAS–induced pancreatic neoplasia.

BACKGROUND AND AIMS: Development of pancreatic ductal adenocarcinoma (PDAC) is a multistep process intensively studied; however, precocious diagnosis and effective therapy still remain unsatisfactory. The role for Notch signaling in PDAC has been discussed controversially, as both cancer-promoting and cancer-antagonizing functions have been described. Thus, an improved understanding of the underlying molecular mechanisms is necessary. Here, we focused on RBPJ, the receiving transcription factor in the Notch pathway, examined its expression pattern in PDAC, and characterized its function in mouse models of pancreatic cancer development and in the regeneration process after acute pancreatitis.

METHODS: Conditional transgenic mouse models were used for functional analysis of RBPJ in the adult pancreas, initiation of PDAC precursor lesions, and pancreatic regeneration. Pancreata and primary acinar cells were tested for acinar-to-ductal metaplasia together with immunohistology and comprehensive transcriptional profiling by RNA sequencing.

RESULTS: We identified reduced RBPJ expression in a subset of human PDAC specimens. Ptf1α-Cre^{ERT}-driven depletion of RBPJ in transgenic mice revealed that its function is dispensable for the homeostasis and maintenance of adult acinar cells. However, primary RBPJ-deficient acinar cells underwent acinar-to-ductal differentiation in ex vivo. Importantly, oncogenic KRAS expression in the context of RBPJ deficiency facilitated the development of pancreatic intraepithelial neoplasia lesions with massive fibrotic stroma formation. Interestingly, RNA-sequencing data revealed a transcriptional profile associated with the cytokine/chemokine and extracellular matrix changes. In addition, lack of RBPJ delays the course of acute pancreatitis and critically impairs it in the context of KRAS^{G12D} expression.

CONCLUSIONS: Our findings imply that downregulation of RBPJ in PDAC patients derepresses Notch targets and promotes KRAS-mediated pancreatic acinar cells transformation and desmoplasia development. *(Cell Mol Gastroenterol Hepatol 2023;16:783–807; https://doi.org/10.1016/j.jcmgh.2023.07.013)*

Keywords: Acinar Cells; ADM; PDAC.

Pancreatic ductal adenocarcinoma (PDAC) is considered as one of the most deadly diseases due to the aggressiveness and extremely poor prognosis.[1] Currently, almost all therapeutic approaches show very low response rates and have only modest influence on the survival and life quality of the patients. Development of PDAC is a multistage process wherein $Kras^{G12D}$ mutation is the predominant driver mutation and a hallmark of this cancer entity.[2] As a result, acinar cells de-differentiate into a precursor state through acinar-to-ductal metaplasia (ADM), allowing cellular expansion and thereby promoting pancreatic intraepithelial neoplasia (PanIN) lesion formation.[3] With the accumulation of additional mutations (eg, in the genes for INK4A, TP53, or SMAD4) and re-activation of embryonic signaling pathways like Notch signaling, PDAC ultimately emerges from these precursor lesions.[2,4]

The evolutionary conserved Notch pathway comprises 4 receptors (Notch1–4) and 5 ligands (Jagged1, Jagged2, DLL1, DLL3, and DLL4), whereas the basic helix-loop-helix HES and HEY transcription factor families represent the classical Notch target genes.[5,6] Numerous studies have proven that Notch signaling is crucially involved in the development of the pancreas and important for PDAC initiation and progression. Human PanIN and PDAC samples have elevated Notch activity,[4,7] and in the context of mutated KRAS, chronic Notch activation promotes the formation of PanINs as well as their progression, while Notch inhibition by means of a γ-secretase inhibitor significantly reduces the number of lesions.[8,9] In addition, increased expression of Notch signaling components in pancreatic cancer stem cells was shown to promote their maintenance.[10] However, the role of Notch signaling in pancreatic cancer is ambivalent with both, tumor promoting as well as suppressing functions (reviewed in Avila et al).[11,12] In addition, different Notch receptors might have distinct roles for PDAC development.[13]

RBPJ is ubiquitously expressed and importantly, the only immediate transcription factor of the Notch signaling pathway and is essential for regulating Notch target gene expression. RBPJ is able to repress transcription by recruiting corepressor complexes to the promoters of target genes in the absence of any ligand-Notch receptor interaction. On the other hand, Notch target genes are activated upon ligand binding, subsequent Notch receptor cleavage, nuclear translocation of the Notch intracellular domain (NICD)[14] and RBPJ-NICD coactivator recruitment.

Notably, RBPJ also influences pancreas development in a Notch-independent manner. In early pancreatic organogenesis RBPJ interacts with PTF1α, thereby initiating the transcription of its paralogue RBPJL.[15] RBPJL then gradually replaces RBPJ in the PTF1α complex, allowing RBPJ to act in a Notch-dependent manner in the regulation of endocrine cell fate decisions.[16,17] In contrast, the PTF1α-RBPJL complex autoregulates its own expression and drives acinar lineage differentiation and terminal maturation. Accordingly, depletion of RBPJL results in a partial loss of acinar cells and in reduced levels of functional digestive enzymes but surprisingly does not impair the overall viability of the mice.[16] The lack of RBPJL and thereby its PTF1α-related functions was proposed to be compensated by RBPJ in the adult, however, with limited efficiency.[16]

The knockout of the *Rbpj* gene causes massive developmental defects leading to an lethal embryonic phenotype.[18] Pancreas-specific RBPJ deficiency induced during embryonic development by the PTF1α-Cre driver resulted in temporally compromised acinar cell differentiation and abnormal ductal structures, indicating an important role of RBPJ in acinar vs ductal cell fate decision during embryogenesis.[19] Because PDAC develops through an "embryonic-like" stage, the question remains whether RBPJ regains a function in that context.[19] Importantly, loss of RBPJ was already found in many human solid tumors, including pancreatic cancer,[20] and in breast cancer, RBPJ loss was associated with an aggressive tumor phenotype.[20] Nevertheless, the detailed role of RBPJ for PanIN and PDAC development in the adult organism is still unclear. Therefore, both, the function of RBPJ as prime executing factor in Notch signaling as well as its critical participation in the PTF1α complex needs to be addressed. For this, we established conditional mouse models allowing the acinar-specific deletion of the *Rbpj* gene to determine the functional outcome of RBPJ deficiency on pancreas homeostasis in the adult organism. Furthermore, we combined this mouse model with oncogenic $KRAS^{G12D}$ expression to decipher the role of RBPJ inactivation for the initiation of pancreatic neoplasia and for the course of acute pancreatitis (AP).

Results

Loss of RBPJ Is Frequently Found in Human PDAC Patients But Is Not Obviously Associated With the Clinical Outcome

To comprehensively investigate RBPJ expression in human tissue, especially in PDAC, immunohistochemistry (IHC) was performed on 3 independent patient cohorts (human tissue microarrays), in total containing 236 cases of resected PDAC. In the normal adjacent pancreatic tissue (NAT), strong RBPJ staining was observed and these levels were comparable between different patients (Figure 1*A*, *C*, and *E*). In contrast, the overall expression of RBPJ in the

*Authors share co-first authorship.

Abbreviations used in this paper: **ADM, acinar-to-ductal metaplasia; AP, acute pancreatitis; BSA, bovine serum albumin; CSC, cancer stem cell; FCS, fetal calf serum; GSEA, gene set enrichment analysis; HBSS, Hank's Balanced Salt Solution; IHC, immunohistochemistry; IL, interleukin; lncRNA, long noncoding RNA; mRNA, messenger RNA; NAT, normal adjacent tissue; NICD, Notch intracellular domain; PanIN, pancreatic intraepithelial neoplasia; PCA, principal component analysis; PCR, polymerase chain reaction; PDAC, pancreatic ductal adenocarcinoma; qPCR, quantitative polymerase chain reaction; RNA-seq, RNA sequencing; SOM, self-organizing map; TAM, tamoxifen; TBS, Tris-buffered saline; TMA, human tissue microarrays.**

Most current article

2352-345X
https://doi.org/10.1016/j.jcmgh.2023.07.013

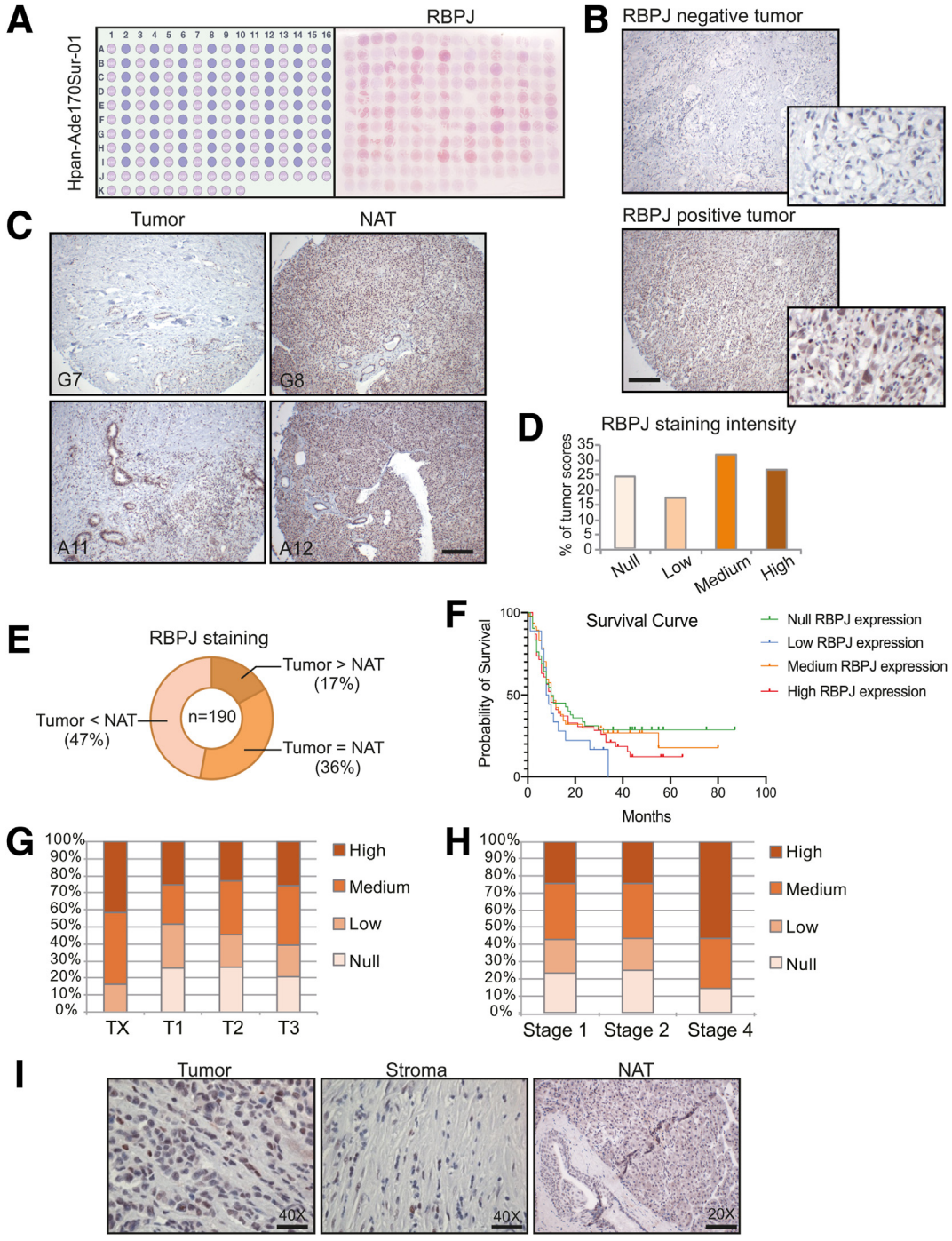

Figure 1. Expression of RBPJ in human PDAC. (*A*) (Left) Schematic representation of a human tissue microarray (TMA) (Hpan-Ade170Sur-01) containing tumor (light purple) and NAT biopsies (purple) from the PDAC patients. (Right) Photograph of the TMA after IHC staining for RBPJ. (*B*) Representative images and magnifications of PDAC specimens with negative and positive RBPJ expression from the TMA cohort. Scale bar represents 200 μm. (*C*) Comparison of the RBPJ expression in PDAC and NAT tissues from 2 patients. The scale bar is representative for all panels and indicates 200 μm. (*D*) Quantification of nuclear RBPJ immunostaining intensity in the TMA PDAC samples. (*E*) Comparison of the RBPJ staining quantification in PDAC and paired NAT tissues. (*F*) Comparison of the overall survival in subcohorts of PDAC patients according to the level of RBPJ expression (null, low, medium, high). RBPJ expression was staged after IHC staining of 2 TMAs containing a total of 162 PDAC samples (HPan-Ade120Sur-01 and HPan-Ade170Sur-01) and differences in patient survival (provided with the TMA) was analyzed by log-rank (Mantel-Cox) test in GraphPad Prism 5.0: $P = .3123$ (null vs high), $P = .3925$ (low vs high), $P = .2428$ (null vs low), $P = .2363$ (low vs medium), $P = .4221$ (medium vs high). (*G*, *H*) Relative RBPJ expression (null, low, medium, and high) stratified by (*G*) tumor size (T) or (*H*) stage of human PDAC tissue specimens from 3 TMAs (n = 236 PDAC samples). (*I*) Comparison of RBPJ expression in PDAC (left), stroma (middle), and NAT (right) tissues from the same patient. Scale bars represent 100 μm (20×) and 50 μm (40×).

PDAC area was markedly decreased and showed a high inter- and intrapatient heterogeneity (Figure 1*B*). In the majority of the cases, the tumor stroma contained only a small number of RBPJ-positive cells. For the tumor specimen itself, 27% and 32% of the cases showed strong or medium RBPJ expression, respectively, while 17% presented with weak staining and, importantly, 24% showed no RBPJ expression at all (Figure 1*D*). When we compared the individual staining intensity in tumor area vs NAT of each patient, we found a stronger (tumor > NAT) or equally strong RBPJ expression in the tumor (tumor = NAT) of 17% and 36% of cases, respectively. A lower staining intensity in the PDAC area (tumor < NAT) was evident in 47% of the patients (Figure 1*E*). However, there were no significant differences between a low and a high RBPJ expression cohort in terms of overall survival (Figure 1*F*). Most of the cases are patients with stage T2 (61.5%) and T3 (26.4%) PDAC. Among those, approximately 40% of the specimen exhibit no or low RBPJ expression (Figure 1*G*). However, there is no clear correlation between RBPJ expression and tumor grade. Similar results were also found in PDAC patients in stage 1 and stage 2 (Figure 1*H*). Both, the no and low RBPJ expression groups have approximately the same percentage as the medium- or high-expression groups. In addition, only 11 cases with metastases were found. Of these, 2 of 11 belong to the low RBPJ expression group.

In conclusion, RBPJ is downregulated in around 40% of the PDAC patients, not only in the tumor compartment, but also in the stroma (Figure 1*I*, middle) compared with NAT (Figure 1*I*, right). There is no obvious correlation between RBPJ expression and overall clinical outcome of the patients.

Acinar-Specific RBPJ Inactivation Does Not Affect Pancreas Morphology

RBPJ is ubiquitously expressed in the pancreas, although it was shown to be more important for endocrine pancreas function in the adult organism.[17] Pancreas-specific deletion of RBPJ during pancreatic development showed an increase of ductal-like structures,[19] suggesting that RBPJ may regulate ADM, a critical process in the formation of PanIN.

To avoid such developmental alterations, we combined *Rbpj*$^{flox/flox}$[21] and *Ptf1α-Cre*^{ERT} mouse lines[22] to generate the conditional *Ptf1α-Cre*$^{ERT/+}$; *Rbpj*$^{flox/flox}$ model hereafter referred to as iCR mice (Figure 2*A*). Six- to 8-week-old iCR mice were used for tamoxifen (TAM)-dependent deletion of *Rbpj*, thus allowing the investigation of consequences on the adult acinar cell homeostasis and pancreatic tumorigenesis. Analysis was performed at different time points (12, 28, 36, and 48 weeks) after TAM administration (Figure 2*C*). RBPJ was successfully deleted in the acinar compartment as determined by polymerase chain reaction (PCR) and IHC (Figure 2*B* and *D*). We did not see any obvious alterations in the growth rate (Figure 2*E*) and morphology at the different time points. Therefore, we selected the latest time point (ie, 48 weeks after TAM treatment) for further analysis (Figure 3*A*).

RBPJ was successfully deleted in the acinar compartment as determined by IHC using an RBPJ-specific antibody at 48 weeks after TAM application (Figure 3*B*, right). Importantly, ductal cells and the islets of Langerhans still exhibited RBPJ staining confirming the acinar specificity of our conditional mouse model. Hematoxylin and eosin staining revealed no gross morphological alterations in iCR mice compared with control animals (Figure 3*B*). Although our model system is heterozygous for *Ptf1α* due to the knock-in of the Cre recombinase gene in the *Ptf1α* locus, which might lead to *Ptf1α* haploinsufficiency, the protein was readily expressed in acinar cells, underlining that cell identity is not disturbed by the additional loss of RBPJ in the iCR TAM-treated group. Likewise, also amylase staining of iCR mice revealed no alteration compared with control animals. In addition, there were no major differences in ductal (CK19) and endocrine (insulin) compartment of iCR mice (Figure 3*B*). Quantitative PCR (qPCR) analyses of total pancreas showed slightly but not significantly reduced expression of acinar markers (*Rbpjl*, *Cela1*, *Cpa1*, and *Ctrb1*) (Figure 3*C*).

In summary, the loss of RBPJ in the context of PTF1α haploinsufficiency is not sufficient to initiate the development of pancreatic lesions or gross histological alterations. Thus, RBPJ function is most probably dispensable for steady-state pancreas homeostasis in the adult.

RBPJ-Deficient Pancreatic Acinar Cells Induce ADM Ex Vivo

To test the hypothesis that loss of RBPJ function primes acinar cells for transformation events, primary acinar cells were isolated from the iCR transgenic mice and were subjected to 3-dimensional cell culture (Figure 4*A*). Treatment with transforming growth factor α was used as a positive control. After 3 days in culture, acinar cells from iCR but not from the noninduced control animals presented considerable structural changes reminiscent of ADM (Figure 4*B* and *C*). ADM was evident, at every time point after TAM treatment of the mice. The phenotypic changes were accompanied by alterations on the messenger RNA (mRNA) level. Expression of the acinar markers such as *Rbpjl*, *Ptf1α*, and amylase (*Amy2a*) as well as the genes characterizing terminal differentiated cells (*Mist1*, *Nr5a2*, and *Gata6*) were markedly reduced in cells showing ADM (Figure 4*D*). At the same time, the ductal marker *Ck19* was significantly induced (Figure 4*D*). Together, these data argue for a protective function of RBPJ in stress induced acinar cells transformation processes.

RBPJ Deficiency Sensitizes Pancreatic Acinar Cells to Kras-Mediated PanIN Initiation

We determined that RBPJ is dispensable for pancreas homeostasis and maintenance in the adult organism, whereas RBPJ function is critical for the suppression of acinar cell transformation. We therefore anticipated that the combination of oncogenic KRAS^{G12D} expression together with deletion of RBPJ in the adult pancreas would facilitate the progression of ADM to PanIN. For this, we crossed our iCR mice with the LSL-Kras^{G12D} model (iKC, Figure 2*A*) to generate *Ptf1α-Cre*$^{ERT/+}$; *LSL-Kras*$^{G12D/+}$; *Rbpj*$^{flox/flox}$ mice, hereafter referred to as iKCR mice (Figure 2*A*). Upon TAM-dependent Cre recombinase activation both, KRAS^{G12D}

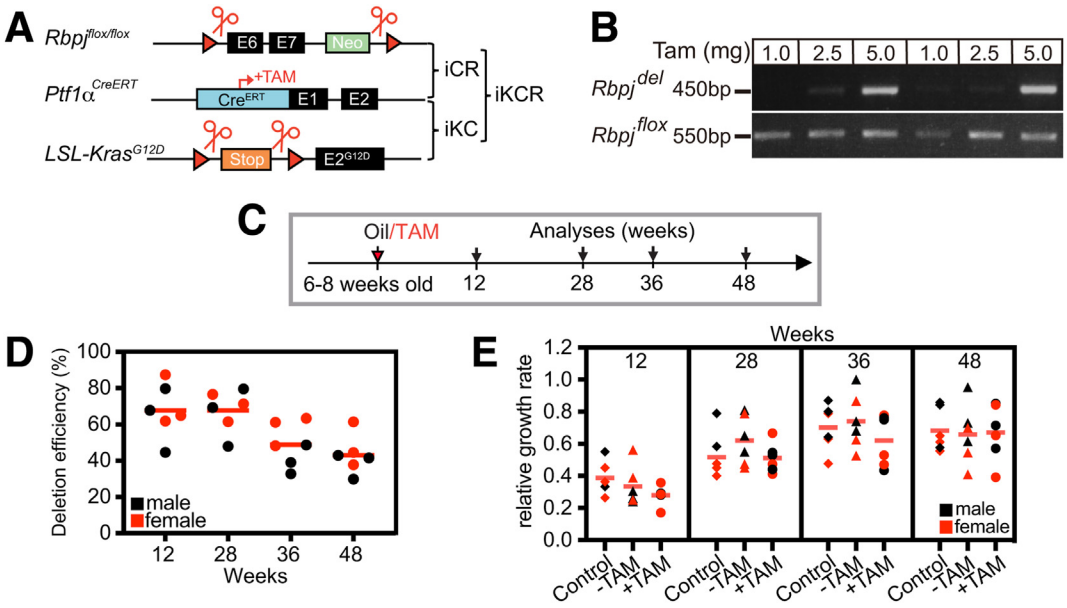

Figure 2. Characterization of iCR mice. (*A*) Schematic genomic organization of the mouse models used in this study. Conditional knockout of RBPJ under control of the Ptf1α promoter in the pancreas (*Ptf1*α*-Cre*^{ERT}*; Rbpj*$^{flox/flox}$ [iCR]) as well as in the context of activated Kras^{G12D} (*Ptf1*α*-Cre*^{ERT}*; Rbpj*$^{flox/flox}$*; Kras*^{G12D} [iKCR]) via the TAM-induced Cre-loxP recombination systems. Upon TAM-mediated Cre^{ERT} activation, the excision of loxP-flanked exons enables deletion of *Rbpj* (iCR) and/or deletion of a stopper element enables the activation of *Kras*^{G12D} expression (iKC or iKCR). (*B*) *Rbpj* deletion PCR. Pancreata were harvested 2 weeks after indicated TAM treatment. DNA isolated from iCR mouse pancreata was analyzed by PCR using primers specific for the *Rbpj*^{del} (amplicon size: 450 bp product) and *Rbpj*^{flox} (550 bp product) allele. PCR products were separated on 1.5% agarose gels. Representative results from 2 mice per group are shown. (*C*) Experimental timeline for analyzing the iCR mouse model. Mice were injected with oil/TAM at the age of 6–8 weeks for 5 consecutive days. Pancreata were harvested 12, 28, 36, and 48 weeks after oil or TAM treatment. (*D*) RBPJ deletion efficiency in the acinar cells was determined by IHC against RBPJ in iCR mice 12, 28, 36, and 48 weeks after TAM injection (n = 6 per group). Quantification was performed by counting RBPJ-negative vs total acinar cell nuclei in 10 different regions of microphotographs. Individual values (as % of total) as well as the mean (red line) are shown. (*E*) Growth rate of control (*Rbpj*$^{flox/flox}$, square) and iCR mice 12, 28, 36, and 48 weeks (w) after vehicle (–TAM) (downright triangle) or TAM (+TAM) (circle) treatment was determined by the equation: R = (G1 – G0)/G0. Each group contains 6 mice. G0: start point weight; G1, endpoint weight; R, growth rate.

expression as well as RBPJ deletion was induced as described previously.

Four weeks after the induction of oncogenic KRAS expression (Figure 5*A*), iKC mice presented mild ADM (0.18 events per mm^2) in the pancreatic tissue. In contrast, iKCR pancreata additionally lacking RBPJ expression (Figure 5*B*) exhibited low-grade PanIN lesions accompanying ADM (0.8 events per mm^2) in the acinar parenchyma (Figure 5*C*). Consistently, these histological alterations were corroborated by an increasing degree of CK19-positive ductal structures displaying faint acinar features (Figure 5*B*). Histology-based lesion grading and quantification in iKCRs compared with iKCs indeed showed a 3-fold and a nearly 10-fold increase in ADM and PanIN-1, respectively (Figure 5*C* and *H*). We also identified increased fibrosis with infiltrating immune cells (Figure 5*B*) and a trend toward more mucin-secreting structures (Figure 5*D* and *E*). Moreover, Ki67 marker analysis revealed sustained mitotic activity in neoplastic cells, indicative of high-risk precursor lesions, as well as proliferative cells within the PanIN-associated stroma denoting an advanced desmoplasia in the iKCR pancreata (Figure 5*B*, *F*, and *G*).

Twelve weeks postinduction (Figure 6*A*), histopathological evaluation of pancreata from iKC mice revealed the presence of scattered low-grade PanIN-1 lesions with prominent RBPJ expression but with minimal proliferative index (Figure 6*B*, *C*, and *G*). Except these rare low-grade neoplastic lesions, iKC pancreatic tissue remained largely inconspicuous without major dysplastic progression over the course of 8 weeks (Figure 6*B* and *C*). In contrast, targeted inactivation of RBPJ led to massive remodeling of the pancreas, leaving almost no healthy tissue, and eventually compromising islet integrity due to extensive premalignant lesion formation (Figure 6*B*). In particular, we observed a predominant increase of not only low-grade PanINs, but also high-grade PanIN-3 lesions in iKCR pancreata compared with iKC counterparts, with no evidence of invasive cancer at this time point (quantification, Figure 6*H*). This rapid progression toward more advanced PanINs was substantiated by the typical histological alterations, including mucin accumulation and a desmoplastic reaction comprising α-smooth muscle actin–positive fibroblasts and dense stromal collagen deposition accounting for 40% of total iKCR pancreatic tissue (Figure 6*B*–*F*). In line, iKCR PanINs showed pronounced mitotic indices (Ki67 staining) correlating with their higher-grade status (Figure 6*C* and *G*).

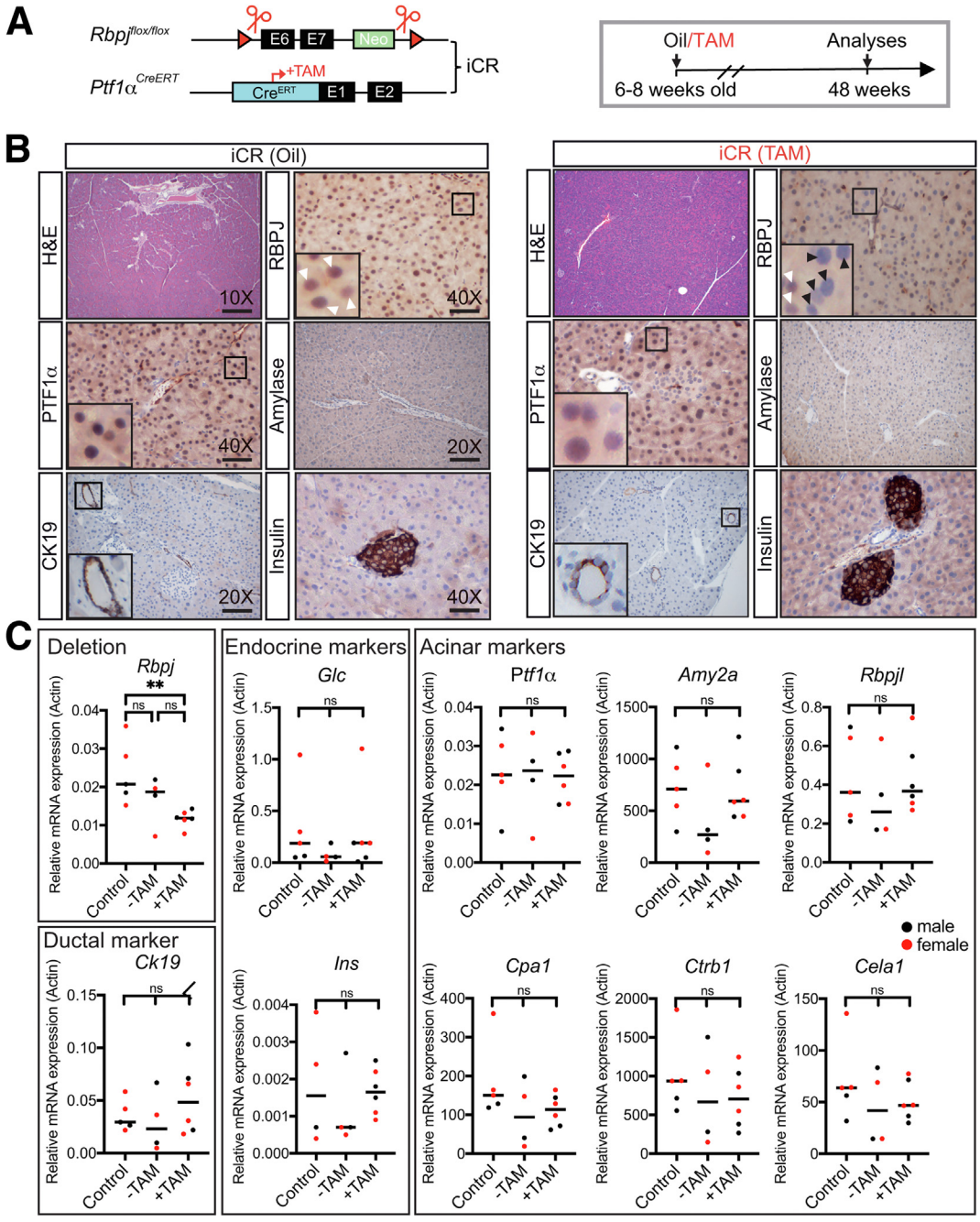

Figure 3. Conditional knockout of RBPJ in the adult mouse pancreas does not alter the overall pancreas morphology. (*A*) (Left) Schematic genomic organization of the mouse models used in this study. Conditional knockout of RBPJ under the control of the Ptf1α promoter in the pancreas (*Ptf1α-Cre^{ERT}; Rbpj$^{flox/flox}$* [iCR]) via the TAM-induced Cre-loxP recombination systems. Upon TAM-mediated Cre^{ERT} activation, the excision of loxP-flanked exons enables deletion of *Rbpj* (iCR). (right) Experimental timeline for analyzing the iCR mouse model. Mice were injected with oil/TAM at the age of 6–8 weeks for 5 consecutive days. Pancreata were harvested 48 weeks after oil treatment or TAM treatment. (*B*) Representative images of tissues stained with hematoxylin and eosin (H&E) or IHC for RBPJ, PTF1α, amylase, CK19, and insulin in iCR pancreata 48 weeks posttreatment with vehicle (black) or TAM (red). Scale bars represent 200 μm (10×), 10 μm (20×), and 50 μm (40×). White and black arrowheads highlight RBPJ-positive and RBPJ-negative nuclei, respectively. Selected regions (box) are magnified in the lower left corner. (*C*) Real-time qPCR (RT-qPCR) analysis in pancreata of iCR mice 48 weeks posttreatment with vehicle (–TAM) (n = 4) or TAM (+TAM) (n = 6). Cre-negative *Rbpj^{floxflox}* mice treated with vehicle were used an additional control group (control) (n = 5). The mRNA samples were analyzed for *Rbpj*, ductal (*Ck19*), endocrine marker (glucagon [*Glc*] and Insulin [*Ins*]), and acinar marker (*Ptf1α, Amy2a, Rbpjl, Cela1*, *Cpa1*, and *Ctrb1*) expression. Individual data as well as the mean (bar) are shown. Unpaired Student's *t* test. $^{**}P < .01$. ns, not significant.

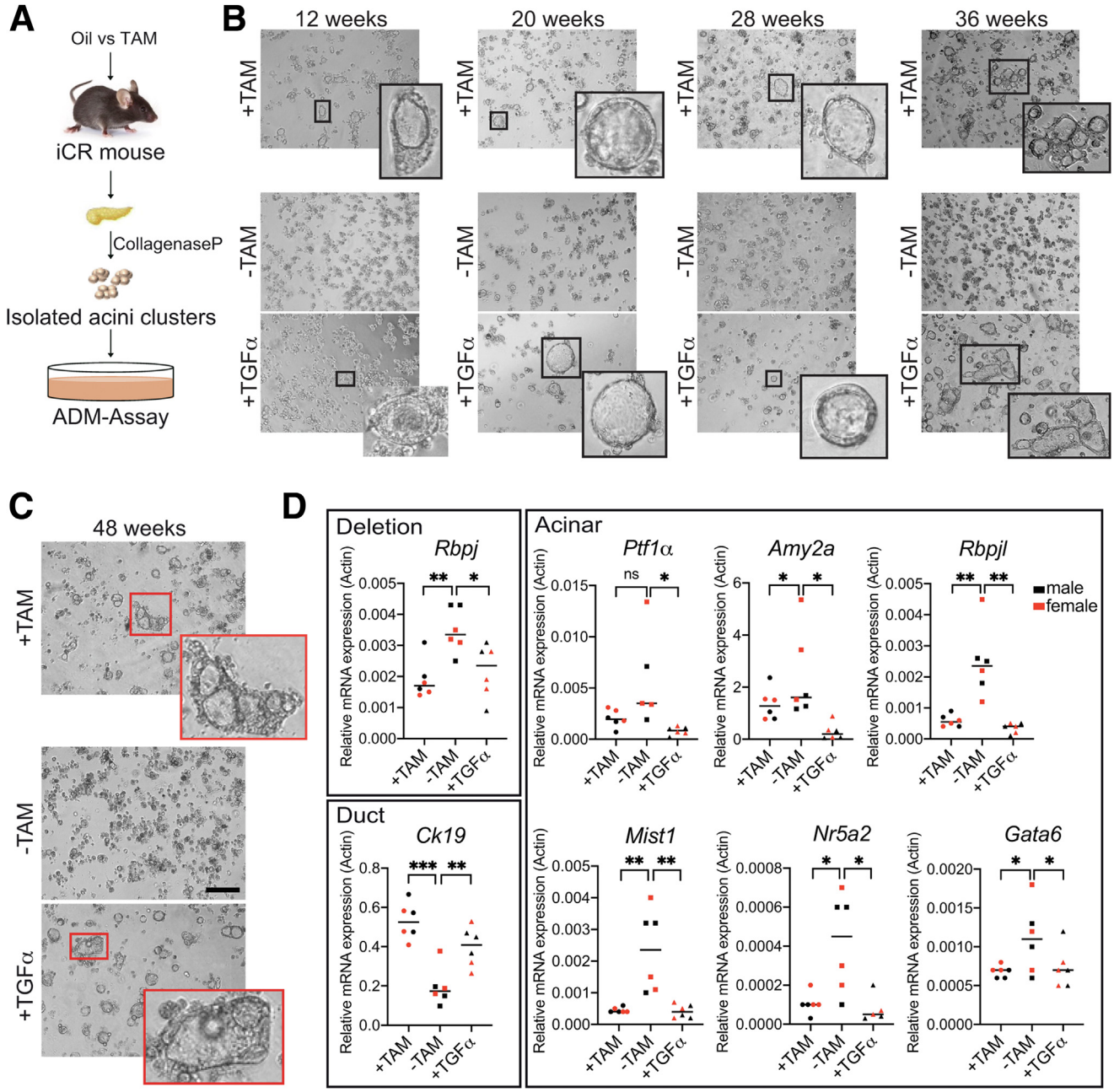

Figure 4. RBPJ-deficient pancreatic acinar cells induce ADM ex vivo. (*A*) Schematic illustration of ex vivo ADM assay with RBPJ-deficient acinar cells. Primary pancreatic acinar cells isolated from TAM-treated iCR mouse were dissociated by collagenase P treatment and finally cultivated in 3-dimensional culture in growth factor–reduced Matrigel. (*B*, *C*) RBPJ-deficient acinar cells induce ADM ex vivo at day 3. Primary acinar cells isolated from iCR mice (*B*) 12, 20, 28, 36, and (*C*) 48 weeks post–TAM (+TAM) and postoil (–TAM) were seeded in growth factor–reduced Matrigel. Acinar cells isolated from oil-treated (–TAM) iCR mice were left untreated or were cocultivated with transforming growth factor α (TGFα) (500 ng/mL) daily for 3 days to induce transdifferentiation (positive control). Inlets on the lower right are magnifications of ductal structures (red box). Scale bar represents 200 μm. (*D*) Real-time qPCR (RT-qPCR) analysis of relative gene expression from the primary acinar cultures at day 3. The total RNA was isolated from 3-dimensional–cultured cells isolated from iCR mice 48 weeks post–TAM (+TAM) treatment and post-oil (–TAM) treatment, and analyzed for *Rbpj* expression as well as ductal marker (*Ck19*) and acinar marker (*Ptf1*α, *Rbpjl, Amy2a, Mist1, Nr5a2, Gata6*) expression (relative to β-*Actin* expression). Individual data from 6 mice as well as the mean (bar) are shown and differences between the groups were analyzed with an unpaired Student's *t* test in GraphPad Prism 5.0. **P* < .05; ***P* < .01; ****P* < .001. ns, not significant.

Taken together, our findings revealed accelerated PanIN initiation and progression upon RBPJ inactivation, strengthening the hypothesis of a tumor suppressive role of RBPJ during pancreas carcinogenesis. Importantly, this implies that the canonical Notch signaling is able to act as a critical repressor of Kras-driven PanIN formation and desmoplasia.

RBPJ Loss Initiates Prominent Gene Expression Changes

To get more insights into the genetic consequences of *Rbpj* inactivation and its tumor-suppressive role, RNA-sequencing (RNA-seq) analysis was performed in the iCR, iKC, and iKCR mice 4 weeks after TAM treatment prior to the onset of major histological alterations (Figures 7 and 8).

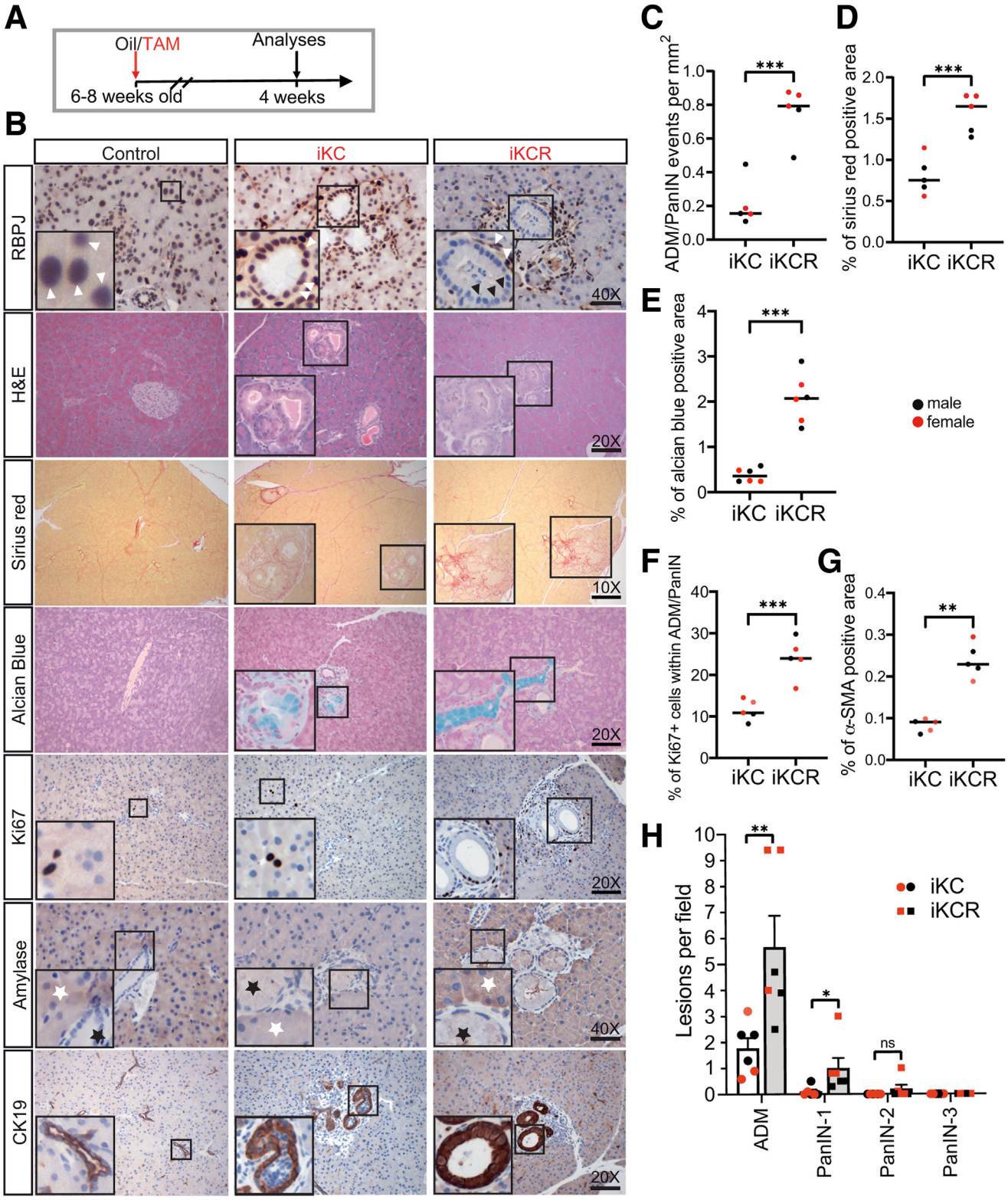

Principal component analysis (PCA) was performed to monitor the overall differential gene expression pattern in the different groups (n = 6 per group, 3 females, 3 males). PCA scatter plots were generated based on mRNA (Figure 7*A*) and long noncoding RNA (lncRNA) (Figure 7*B*). Clearly, TAM- and oil-treated iCR mice clustered close together either based on mRNA or lncRNA, suggesting a nonessential role of RBPJ in the adult acinar cells. TAM- and oil-treated iKCR mice as well as TAM-treated iKC mice formed 3 distinct clusters according to mRNA or lncRNA.

The heatmaps of transcriptome profiling between different groups revealed distinct gene expression patterns that loss of RBPJ induced abundant gene expression, indicating its repressor function (Figure 7*C*–*F*).

Upon *Rbpj* deletion alone (Figure 7*C*), 3 genes were upregulated in acinar cells. Interestingly, *Rhov*,[23] a newly identified PTF1α target, showed a 2.6-fold and a 2.9-fold increase, respectively, in RBPJ-deficient pancreata (Figure 7*C*, Supplementary Table 1) and iKCR mice compared with iKC mice (Figure 7*G*), suggesting a critical role of RBPJ in PTF1α-dependent transcription. RBPJ loss together with oncogenic KRAS expression (iKCR_+TAM) upregulated 77 or 511 genes compared with only RBPJ deficiency (iCR_+TAM) (Figure 7*D*) or the control group (iKCR_–TAM) (Figure 7*E*, Supplementary Table 1), respectively. However, by comparing TAM-treated iCR mice with iKCR mice (iKC_+TAM vs iKCR_+TAM), only 5 genes were found to be differentially regulated (Figure 7*F*) and verified by real-time qPCR analysis (Figure 7*I*). In addition, *Gkn1*, a gene usually overexpressed in early PanIN, was upregulated in iKCR mice prior to massive morphological alterations (Figure 7*H*).

A total of 756 genes were uniquely modulated in iKCR mice treated either with oil or TAM (Figure 7*E*). However, only 5 genes were deregulated when TAM injected iKC and iKCR mice were compared (Figure 7*F*), indicating that major gene expression changes were initiated by oncogenic KRAS expression. Nonetheless, RBPJ loss together with KRAS expression increases the degree of gene dysregulation suggesting a quality change after additional loss of RBPJ expression.

In the presence of oncogenic KRAS expression, qPCR from RBPJ-deficient pancreatic tissue from iKC and iKCR mice revealed a significant increase of *Notch1* and the Notch target genes *Hes1* and *Nrarp* in the iKCR mice (Figure 8*A*). To test whether the genes differentially expressed in the iKC vs iKCR mouse models reflected either as a consequence of RBPJ loss or the consequence of an increased number of ADM/PanIN lesions in the iKCR mice (Figure 7), we used published available expression data from a Kras^{G12D} mouse model.[24] During progression of ADM/PanIN lesions (1-month-old vs 3-month-old mice), there were no changes in gene expression of *Atp10d*, *Ccna1*, *Psap1*, and *Cox18* detectable (Supplementary Table 1). Unfortunately, the noncoding RNA *9430085M18Rik* was not annotated in this dataset. In addition, we also found the Notch-related genes *Notch1* and *Nrarp* (Figure 8*A*) not upregulated in the published dataset. This suggests that most of the genes, differentially expressed in our mouse models (iKC vs iKCR), are indeed a consequence of RBPJ loss. However, because *Hes1* is also upregulated in the dataset form Paul et al (Supplementary Table 1),[24] we cannot exclude that upregulation of *Hes1* is, at least in part, a consequence of increased ADM/PanIN formation in the iKCR mice.

Interestingly, our RNA-seq data revealed that the gene set related to extracellular matrix was dramatically deregulated in the iKC and iKCR group already 4 weeks after TAM treatment (Figure 8*B*–*E*), a time prior to massive stroma formation. The PDAC tumor microenvironment is very heterogenous and provides various biologically active factors like cytokines/chemokines known to promote PanIN development and fibrogenesis.[25,26] Interestingly, we found an enrichment of a large number of collagen-encoding genes after combination of RBPJ loss with oncogenic KRAS^{G12D} expression (iKCR) (Figure 8*B* and *C*, Supplementary Table 2). This was accompanied by an elevated expression of cytokines/chemokines (Figure 8*D* and *E*), including interleukin (IL) family members and C-C motif and C-X-C motif chemokine ligands (Supplementary Table 2). Surprisingly, comparing with the iKC group, the iKCR pancreata presented a downregulation of cell junction maintenance signatures (Figure 8*F*), implying that additional RBPJ loss contributes to loosened cell connections or disturbed of acinar cell organization. Importantly, these alterations even appear prior to the development of significant pancreatic neoplasia, supporting the idea of a suppressive function of RBPJ in PDAC development.

Pancreatic Regeneration Is Delayed Upon RBPJ Deficiency But Impaired in Context of KRAS^{G12D} Expression

Pancreatitis is known as a critical driving force for the development of pancreatic neoplasia, and activation of the Notch signaling pathway was shown to be critical for

Figure 5. (***See previous page***). **RBPJ deficiency sensitizes pancreatic acinar cells to KRAS-mediated PanIN initiation after 4 weeks TAM treatment.** (*A*) Experimental timeline for analyzing the iKC and iKCR mouse models. Mice were injected with oil/TAM at the age of 6–8 weeks for 5 consecutive days. Pancreata were harvested 4 weeks after oil/TAM treatment. (*B*) Representative images of tissues from iKC and iKCR pancreata 4 weeks after oil (black) or TAM (red) treatment stained with hematoxylin and eosin (H&E), Sirius red, Alcian blue, or IHC with antibodies against RBPJ, Ki67, amylase, and CK19. Selected regions (box) are magnified in the left corner. White and black arrow head highlight RBPJ-positive and RBPJ-negative nuclei, respectively. White and black stars represent low and high amylase expression, respectively. Scale bars, 200 μm (10×), 100 μm (20×), and 50 μm (40×). (*C*–*G*) Quantification of (*C*) ADM/PanIN lesions, (*D*) Sirius red–positive stromal area, (*E*) Alcian blue–positive PanINs, (*F*) Ki67-positive ADM/PanIN cells, and (*G*) α-SMA-positive areas in iKC (n = 5) and iKCR (n = 5) pancreata. (*H*) Quantifications of ADM, PanIN-1, PanIN-2, and PanIN-3 lesions 4 weeks post–TAM treatment in iKC (n = 6) and iKCR (n = 6) mice. Data were analyzed with an unpaired Student's *t* test in GraphPad Prism 5.0 and are presented as individual values as well as mean ± SEM (bar). ***$P < .001$. ns, not significant.

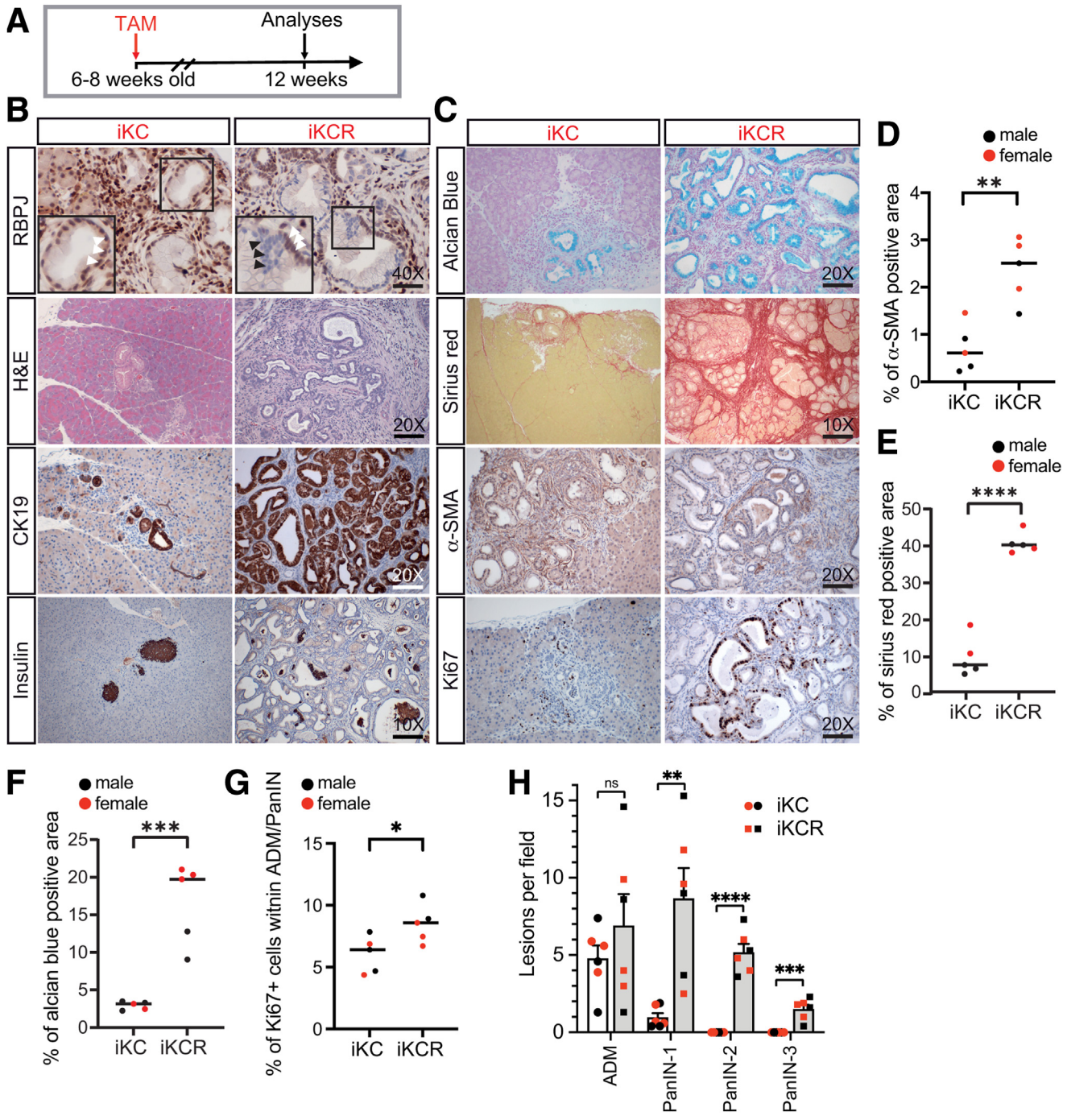

Figure 6. RBPJ-deficient acinar cells accelerate KRAS-mediated PanIN formation 12 weeks post–TAM administration. (*A*) Experimental timeline for analyzing the iKC and iKCR mouse models. Mice were injected with TAM at the age of 6–8 weeks for 5 consecutive days. Pancreata were harvested 12 weeks after TAM treatment. (*B*) Representative images of tissues from iKC and iKCR pancreata 12 weeks after TAM treatment stained with hematoxylin and eosin (H&E) and IHC images of RBPJ, CK19, and insulin in iKC and iKCR pancreata. Selected regions (box) are magnified in the left corner. White and black arrowheads highlight RBPJ-positive and RBPJ-negative nuclei, respectively. (*C*) In the context of $KRas^{G12D}$ expression, RBPJ deficiency dramatically induces fibrotic stroma formation 12 weeks after TAM administration. Representative Alcian blue, Sirius red, and IHC images of α-smooth muscle actin [α-SMA] and Ki67 in iKC and iKCR pancreata 12 weeks after TAM treatment. Scale bars represent 200 μm (10×) and 100 μm (20×). (*D–G*) Quantification of (*D*) α-SMA–positive area, (*E*) Sirius red–positive stromal area, (*F*) Alcian blue–positive PanINs, and (*G*) Ki67-positive ADM/PanIN cells in iKC (n = 5) and iKCR (n = 5) pancreata. (*H*) Quantification of ADM, PanIN-1, PanIN-2, and PanIN-3 lesions in iKC (n = 6) and iKCR (n = 6) mice. Data were analyzed with an unpaired Student's *t* test in GraphPad Prism 5.0 and are presented as individual values as well as mean ± SEM (bar). *$P < .1$; **$P < .01$; ***$P < .001$; ****$P < .0001$. ns, not significant.

regeneration of the pancreas.[27] In addition, AP has the potential to facilitate the progression of precursor lesions.[28] Because inactivation of RBPJ function, even in the context of oncogenic KRAS expression, was not sufficient to initiate pancreatic carcinogenesis during the observation period of the mice, AP was used as an additional triggering factor. For this, cerulein-induced AP was applied to iC, iCR, iKC, and iKCR animals and pancreatic tissue was analyzed at different time points post-AP (Figure 9*A*).

To investigate the immediate inflammatory response, pancreata from the different models were examined 1 day after cerulein injection (for details, see Materials and Methods). Morphological alterations, especially edema formation with vacuolated cytoplasm and prominent immune cell infiltration, were found in iC and iCR mice (Figure 9*B*). The changes in iKCR pancreata compared with iKC showed significant changes, as a sparse additional acinar dilatation was observed. In addition, histopathology of iKCR pancreata showed acinar cells that underwent degranulation and dilatation with partial necrosis. RBPJ loss in iCR and iKCR mice was confirmed by IHC (white arrows), whereas infiltrating immune cells still present a strong RBPJ expression level (Figure 9*B*, RBPJ, black arrows). In all mouse models, the acinar cells underwent acinar-to-ductal reprogramming/ADM, resulting in tubular structures with increased CK19 expression (Figure 9*B*, CK19; quantification shown in Figure 9*C*). Cerulein-induced AP mostly affects the acinar cells, which therefore represent the main cell population proliferating upon tissue regeneration; however, Ki67 positive cells were also detected in the periphery of acinar-to-ductal reprogramming/ADM regions (Figure 9*B*, Ki67). Quantification of the pancreatitis score 1 day after cerulein treatment is shown in Figure 9*D*.

The pancreatic regeneration was analyzed in iC and iCR mice 7 days after cerulein administration not only with mostly re-established parenchymal tissue and reduced edema, but also with partially remaining necrosis and infiltrating immune cells, although significantly reduced in numbers. In strong contrast, iKC and iKCR mice did not show signs for regeneration: inflammation and necrosis persisted in both mouse models (Figure 10, hematoxylin and eosin). In addition, RBPJ-positive cells were also found in the peripheral regions of iCR and iKCR mice representing inflammatory cells (Figure 10, RBPJ). CK19 staining marked the ADM lesions that locally remained in pancreata of iC and iCR mice in lobes with a high infiltration of immune cells. In iKC and iKCR pancreata, the ADM process even progressed (Figure 10, CK19). During pancreatic refinement, Ki67-positive cells were dramatically increased in all mouse models and are located in the necrotic compartment, the peripheral region as well as acinar cells and duct-like structures (Figure 10, Ki67). Gene expression analyses by qPCR from pancreata of iC, iCR, iKC, and iKCR mice showed gradually loss of exocrine markers *Amy2a2, Ptf1α,* and *Rbpjl* (Figure 11*A*), but ductal marker *Ck19* and fibrosis markers *Fn1* and α-smooth muscle actin (*Acta2*) showed the opposite direction (Figure 11*B*). Quantifications of the pancreatitis score show significant differences between iC and iCR mice (Figure 11*C*). Surprisingly, the pancreatitis-induced PanINs occurring in iKC and iKCR mice develop different mucin phenotypes (Figure 10, Alcian blue staining). Mucins in iKC mice were either located in the cytoplasm of ductal-like structures or in the stroma, whereas mucins in iKCR mice were predominantly located in the cytoplasm of PanIN cells. To further investigate the different mucin expression profiles, real-time qPCR analyses was performed. Interestingly, *Muc4* and *Muc6* were upregulated in iKCR pancreata compared with that of iKC mice, while *Muc1* and *Muc5ac* were downregulated. However, the difference in *Muc5ac* expression was not significant between the 2 groups (Figure 11*D*). Nonetheless, all pancreatic desmoplasia were embedded in collagenic fibrosis (Figure 10, Sirius red).

Typically, cerulein-induced AP is refined 7 days after induction,[29] and pancreatic tissue is almost completely recovered in wildtype mice after 3 weeks. However, analyzing iC, iCR, iKC, and iKCR mice at this time point (Figure 12) revealed different outcomes. The pancreas was completely regenerated in iC mice, whereas loss of RBPJ, delayed the pancreatic regeneration process leaving local necrotized acini in iCR mice. However, both iKC and iKCR mice showed no pancreatic tissue repair at all, but instead the lesions occurring in these mice even further progressed into high grade PanINs. CK19-expressing ductal structures presented normally in appearance and number in iC and iCR mice. In iKC and iKCR mice, the pancreatic tissue still mainly consists of ADM lesions, partial duct dilatation, and persistent progression of PanINs. The number of proliferative cells returned to a normal level in the iC and iCR acinar compartment as assessed by Ki67 staining. Only a few Ki67-positive cells were found in the necrotic area of iCR mice. We identified more proliferative cells in iKC and iKCR pancreata, which preferentially located in ADM lesions or duct-like structures, but also very few cells were found in the peripheral region (Figure 12).

Discussion

RBPJ participates in the PTF1α-complex essential for pancreatic development and is the central regulation platform for Notch signaling, which was shown to be involved in pancreatic cancer initiation and progression. We determined that RBPJ is frequently downregulated in the PDAC patients (Figure 1) and therefore performed an in-depth functional characterization of RBPJ in mature acinar cells, pancreatic cancer development, and regeneration after cerulein-induced AP.

RBPJ in Adult Acinar Cells

For acinar lineage specification, there are 3 essential elements: PTF1α, RBPJ, and its paralogue RBPJL.[30] The PTF1α-RBPJ complex is pivotal for RBPJL induction in the early developmental stage, whereas the PTF1α-RBPJL complex is essential for the expression of digestive enzyme genes and terminal differentiation of acinar cells.[15,16] Homozygous deletion of PTF1α in mature acinar cells was shown to be sufficient for reprograming these cells into ductal-like cells[31] and PTF1α inactivation in elastase expressing cells initiated endoplasmic reticulum

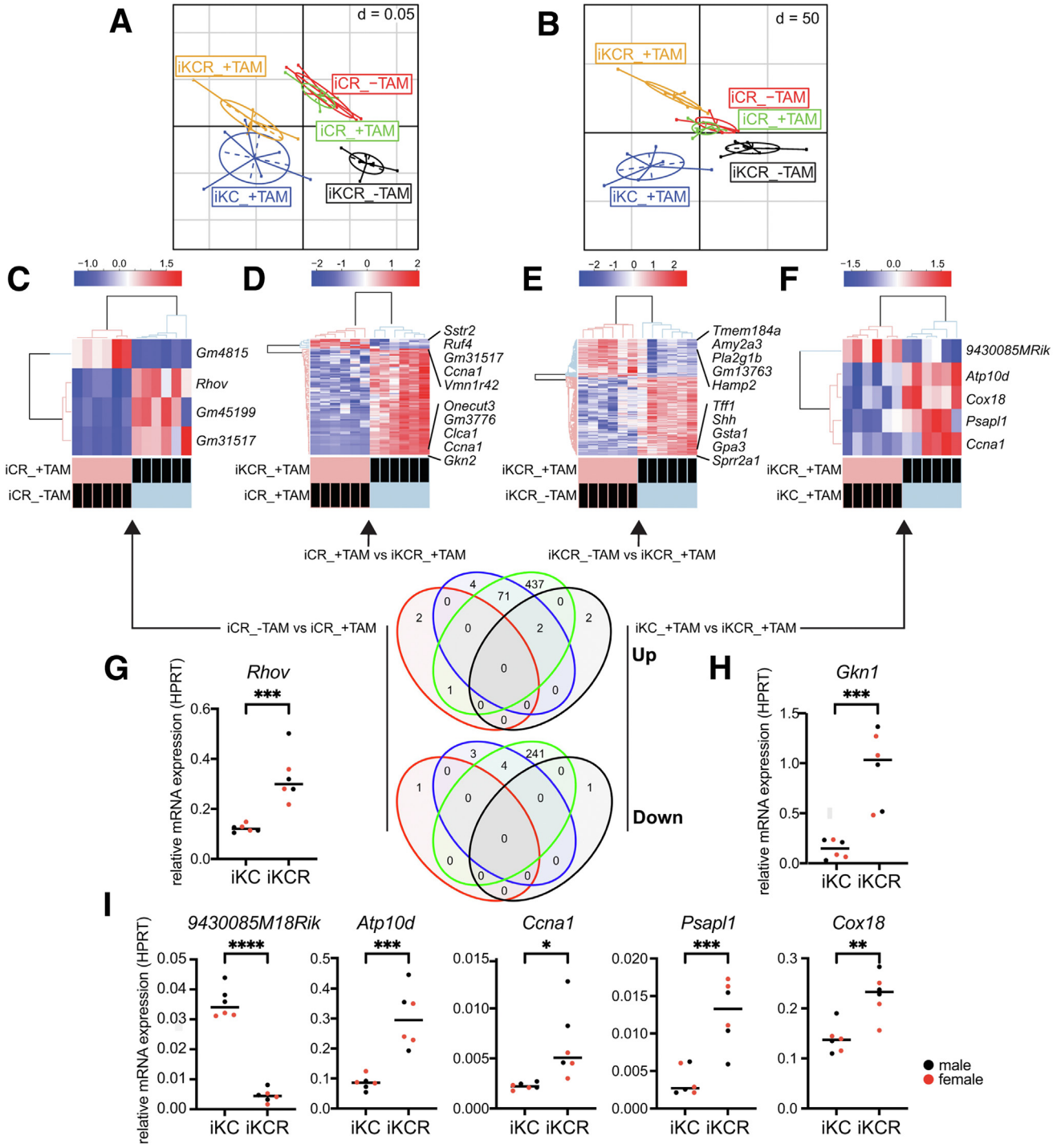

Figure 7. RNA-seq expression profiles of RBPJ-deficient pancreata. Total RNA was extracted from individual mouse models (n = 6 per group, 3 males and 3 females), sequenced, and analyzed as described in Materials and Methods. (*A*, *B*) PCA based on the group analysis plot from RNA-seq data of (*A*) mRNA and (*B*) lncRNA. iCR mice treated with oil (–TAM) and TAM (+TAM) are highlighted in red and green. iKCR mice treated with oil (–TAM) and TAM (+TAM) are highlighted in black and orange. iKC mice treated with TAM (+TAM) are highlighted in blue. (*C*–*F*) (Top) Heatmaps of differentially expressed genes in pancreata obtained from iCR mice treated with oil vs (*C*) TAM, (*D*) TAM-treated iCR mice vs iKCR mice, (*E*) iKCR mice treated with oil vs TAM, and (*F*) TAM-treated iKC mice vs iKCR mice with a significant difference (adjusted *P* value <.05). The color scale based on the row *Z* score is shown at the top. (Bottom) Venn diagrams showing upregulated vs downregulated genes and the overlap between different indicated comparison groups: iCR mice treated with oil vs TAM (red), TAM-treated iCR mice vs iKCR mice (blue), iKCR mice treated with oil vs TAM (green), and TAM-treated iKC mice vs iKCR mice (black). (*G*–*I*) Validation of statistically significant differential gene expression in comparison group of iKCR and iKC pancreata. Data were analyzed with an unpaired Student's *t* test in GraphPad Prism 5.0 and are presented as individual values as well as mean (bar). **P* < .1; ***P* < .01; ****P* < .001; *****P* < .0001. ns, not significant.

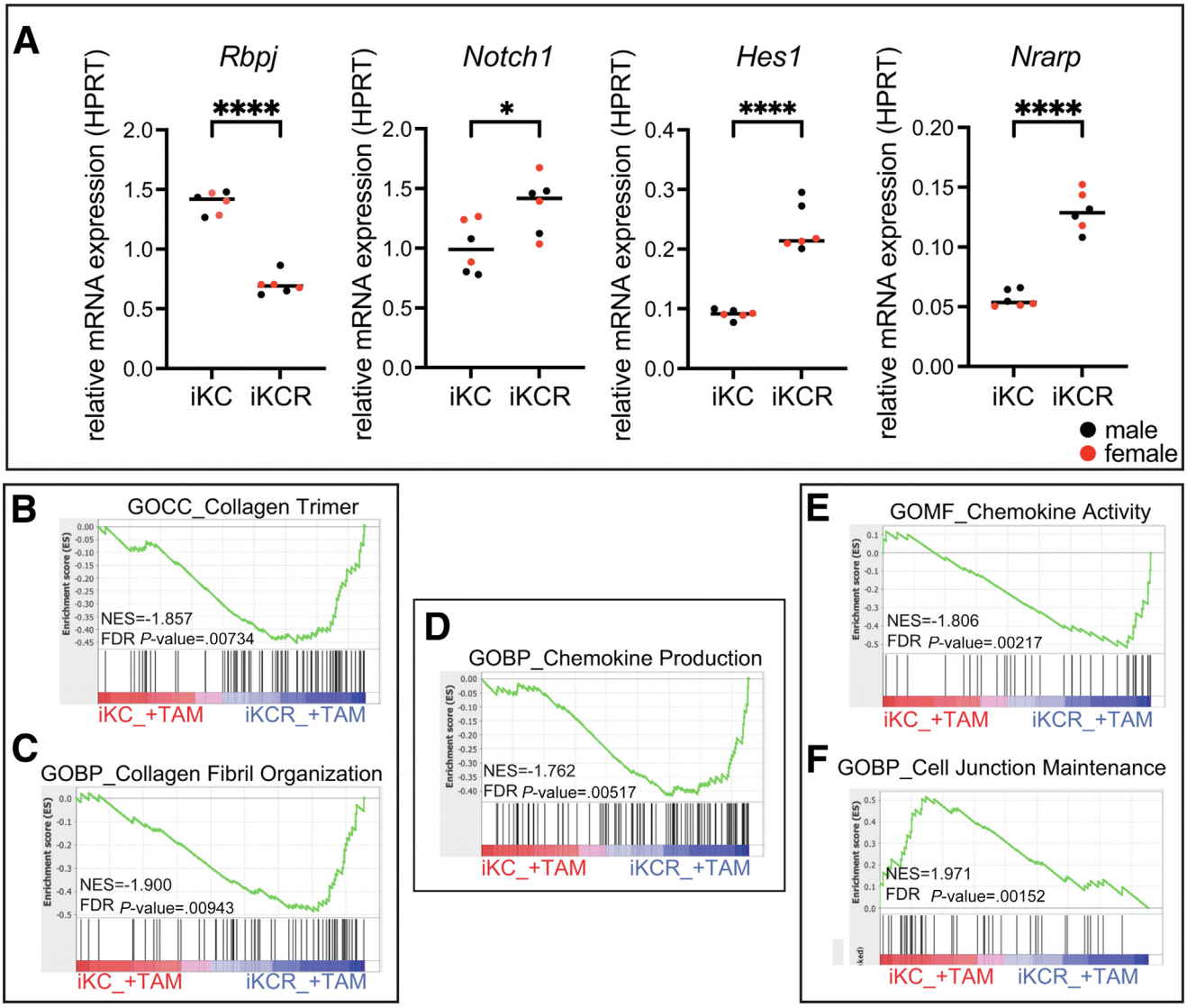

Figure 8. Significantly differential gene expression in iKC and iKCR pancreata. Each group contains 3 males and 3 females. (*A*) Real-time qPCR analysis of Rbpj and Notch-related genes (Notch1, Hes1, and Nrarp) in iKC and iKCR mice. Data were analyzed with an unpaired Student's *t* test in GraphPad Prism 5.0 and are presented as individual values as well as mean (bar). *$P < .1$, ****$P < .0001$. (*B–E*) GSEA of (*B*) collagen trimer, (*C*) collagen fibril organization, (*D*) chemokine production, (*E*) chemokine activity, and (*F*) cell junction in TAM-treated iKC and iKCR pancreata. FDR, false discovery rate; NES, normalized enrichment score.

stress–mediated acinar cell apoptosis resulting in pancreatic volume reduction.[32] Upon global deletion of RBPJL, RBPJ was able to partially compensate RBPJL function in the PTF1α complex.[16] Besides RBPJ/RBPJL, NR5A2 and MIST1 are additional essential acinar marker proteins. Nr5a2 haploinsufficiency in the adult pancreas does not result in gross histological alterations, while Nr5a2 knockout mice develop pancreas atrophy and local ductal lesions.[33] Similarly, Mist1 knockout mice show a severely disorganized pancreas and decreased acinar cell numbers. This phenotype could be rescued by reintroduction of MIST1.[34,35]

In contrast, RBPJ-deficient acinar cells lack obvious phenotypical alterations (Figure 3) and showed no significant changes in acinar marker gene expression (Figure 3*C*). This suggests that RBPJ is not the key factor for homeostasis and maintenance of mature acinar cell function and identity. Surprisingly, ex vivo cultivation of primary acini of iCR mice triggered the transition from an acinar to a ductal phenotype (Figure 4). This supports the idea that additional stress factors are able to change the differentiation status of acinar cells in the absence of RBPJ function, and possibly pancreatitis could be such an additional stress factor in vivo.

RBPJ is the DNA-binding component of the Notch signaling pathway that either interacts with corepressors to downregulate gene expression or recruits coactivators to activate target gene transcription. The Notch target gene *Hes1* was shown to be vital for pancreatogenesis by influencing the pancreatic epithelial precursors population, while NOTCH1 and NOTCH2 function is dispensable for pancreatic development,[36] Terminally differentiated acinar cells do not

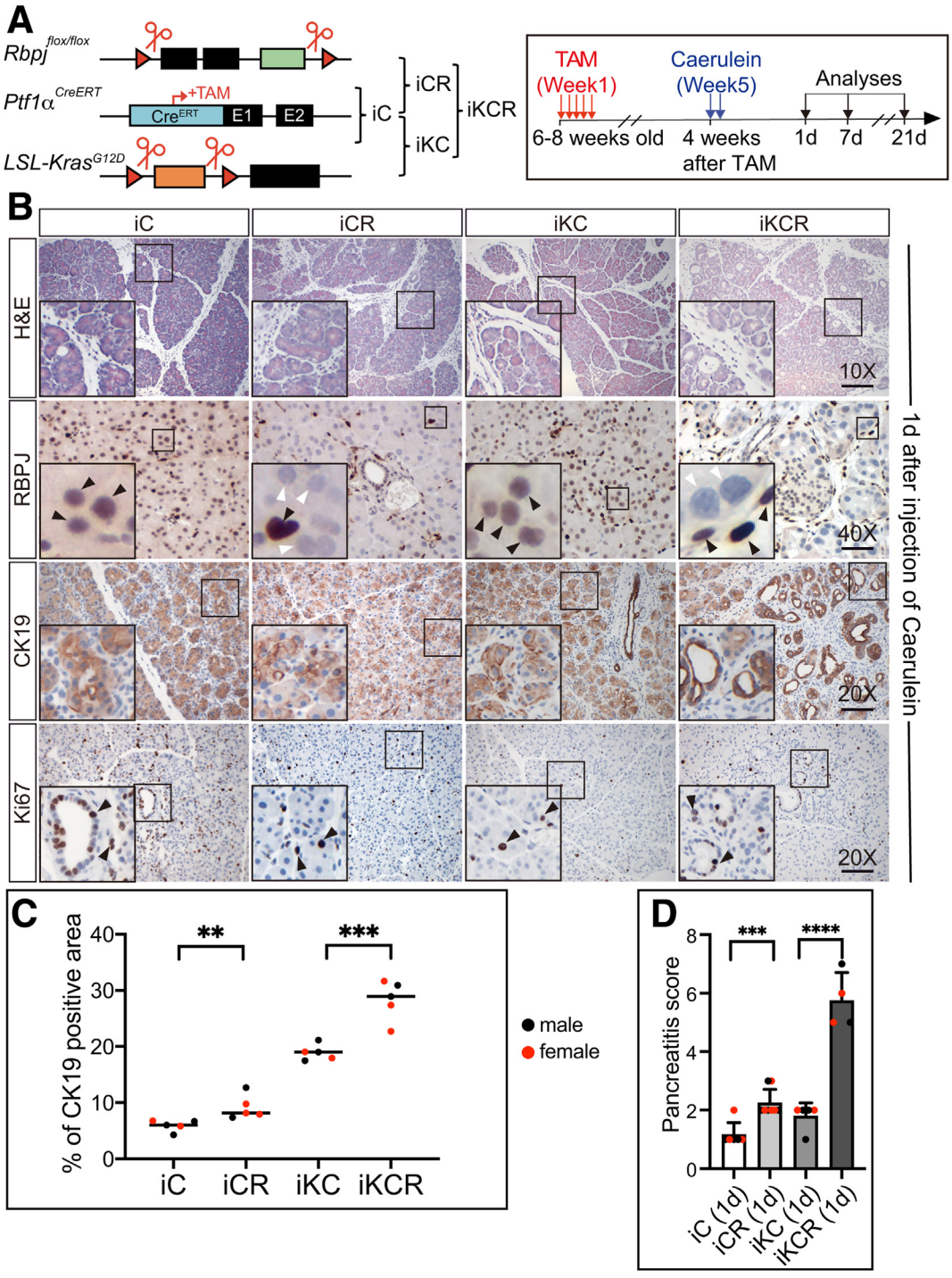

Figure 9. (Immuno)histological staining of pancreata from iC, iCR, iKC, and iKCR mice 1 day after cerulein-mediated induction of AP. (*A*) (Left) Illustration of the experimental design for analyzing the iC, iCR, iKC, and iKCR mouse models. (Right) Mice were injected with TAM at the age of 6–8 weeks for 5 consecutive days (week 1). Subsequently, mice were injected with cerulein at week 5 for 2 consecutive days (8-hourly injections) to induce AP. Pancreata were harvested 1, 7, and 21 day(s) after the last treatment. (*B*) Representative images of pancreata from iC, iCR, iKC, and iKCR mice stained with hematoxylin and eosin (H&E) and IHC with antibodies against RBPJ, CK19, and Ki67. Magnifications of selected regions are shown in the left corner. Black and white arrows indicate RBPJ/Ki67-positive and RBPJ-negative cells. One day after the last treatment with cerulein pancreata were harvested (6 mice per group, 3 males and 3 females). Scale bars represent 200 μm (10×), 100 μm (20×), and 50 μm (40×). (*C*) Quantification of CK19-positive area in pancreata from iC (n = 5), iCR (n = 5), iKC (n = 5), and iKCR (n = 5) mice. (*D*) Quantification of the pancreatitis score as described in the Materials and Methods 1 day after the last treatment with cerulein. Data were analyzed with an unpaired Student's *t* test in GraphPad Prism 5.0 and are presented as individual values as well as mean ± SEM. $^{**}P < .01$; $^{***}P < .001$; $^{****}P < .0001$.

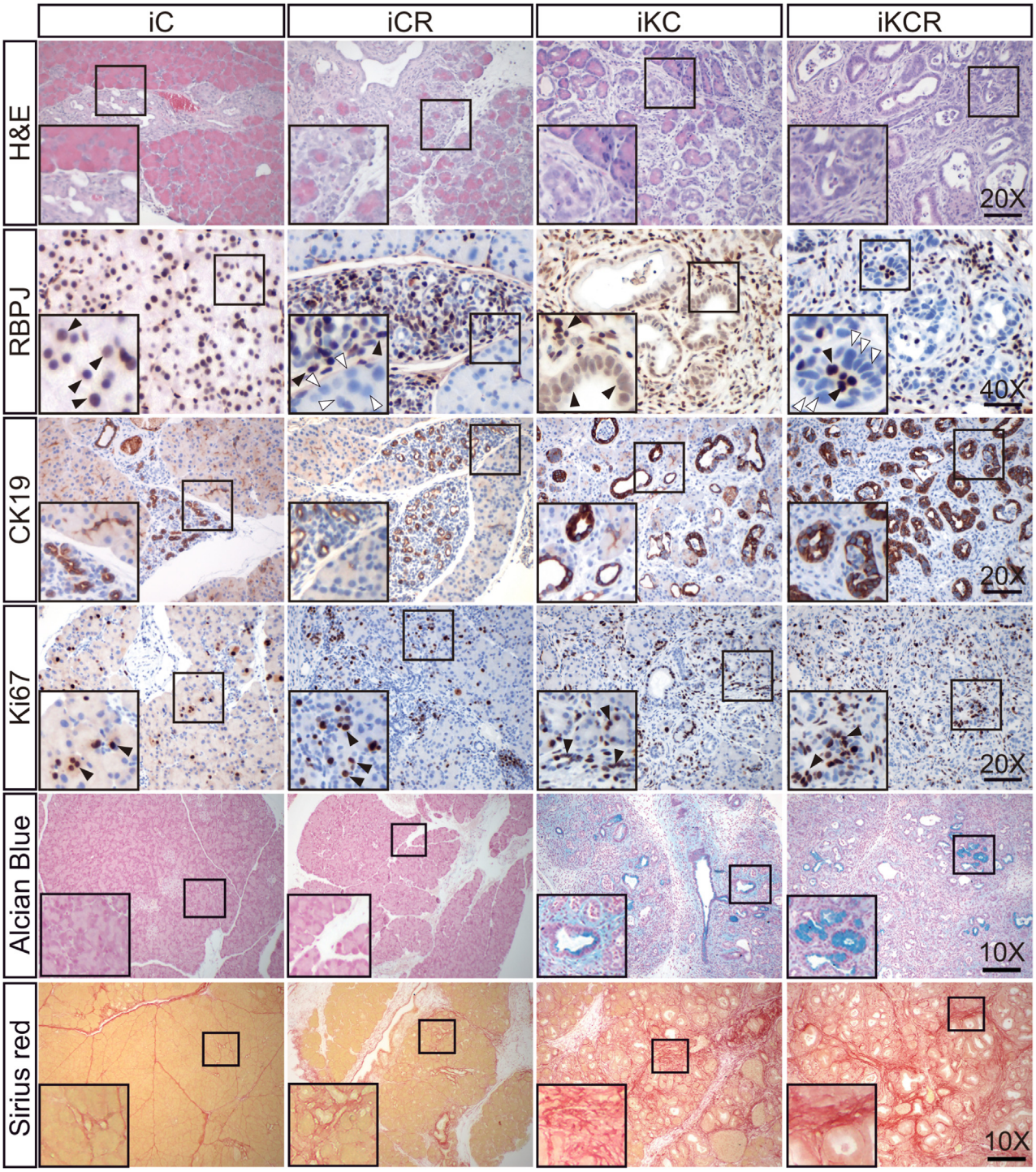

Figure 10. (Immuno)histological staining of pancreata from iC, iCR, iKC, and iKCR mice 7 days after cerulein-mediated induction of AP. Representative images of pancreata from iC, iCR, iKC, and iKCR mice stained with hematoxylin and eosin (H&E) and IHC with antibodies against RBPJ, CK19, and Ki67 as well as Sirius red and Alcian blue. Magnifications of selected regions are shown in the left corner. Black and white arrows indicate RBPJ/Ki67-positive and RBPJ-negative cells, respectively. Scale bars represent 200 μm (10×), 100 μm (20×), and 50 μm (40×).

express Notch1, Notch2, and Hes1 and thus are neglectable for the maintenance and homeostasis of the exocrine pancreas.[36] Therefore, RBPJ most likely inhibits gene expression in mature acinar cells when active NOTCH is absent.

Based on these findings, we assume that (1) RBPJ is not the master regulator for acinar cell maintenance and homeostasis in the adult state and (2) RBPJ is able to prevent the acinar-to-ductal cell differentiation upon additional

triggers. However, it is not sufficient to transform mature acinar cells.

RBPJ Loss in Context of KRAS Expression

The oncogenic *Ras* mutation is the key driver of pancreatic cancer development and is present in approximately 94% of PDAC patients. Among these over 40% are $KRAS^{G12D}$ mutations,[37] and conditional $KRAS^{G12D}$ mouse models are able to drive acinar cell transformation and do sufficiently recapitulate PDAC development.[38,39] Interestingly, during PanIN progression and in the presence of pancreatitis, the shift from acinar to ductal cell identity is accompanied by a gradual decline in PTF1α and RBPJL expression.[29] Overall, RBPJ expression appears to be heterogeneous in different murine PDAC cell lines.[29] Remarkably, we observed concomitant RBPJ expression also in infiltrating immune cells and fibroblasts (Figures 5*B* and 6*B*).

Notch components are frequently upregulated in PanINs and PDAC.[7,36] In this study, we did not detect significant induction of Notch target gene (eg, *Hes1*) or Notch component (eg, *Notch1*) expression in iCR mice. RBPJ deficiency in combination with $KRAS^{G12D}$ led to an upregulation of *Notch1*, *Nrarp*, and *Hes1* 4 weeks after TAM treatment as detected by qPCR (Figure 8*A*), implicating a transcriptional repressor function of RBPJ in PanIN initiation. However, because induction of *Hes1* was also shown in a $KRAS^{G12D}$ mouse model without RBPJ deletion (see Supplementary Table 1),[24] we cannot exclude the possibility that *Hes1* transcriptional activation, at least in part, results from enhanced ADM/PanIN formation independent of RBPJ loss in the iKCR mice compared with the iKC mice. It was shown that the overexpression of NICD, the active form of the Notch receptor, is able to override the repressive RBPJ function and enhanced KRAS-driven PanIN initiation. In contrast, *Notch1* deletion suppresses oncogenic KRAS-induced PanIN formation.[38,40] A similar outcome was found in *Hes1* knockout mice in which loss of HES1 inhibits PanIN formation in the KRAS-expressing pancreata.[36] Therefore, NOTCH1 and HES1 are considered as oncogenic factors in pancreatic cancer development. Indeed, ablation of RBPJ sensitizes cells to KRAS-driven acinar cell transformation with acceleration of PanIN progression compared with KRAS activation alone (Figures 5 and 6). The mRNA for RHOV was also upregulated after RBPJ loss (Figure 7*C* and *G*). RHOV is a member of the cdc42 family of small GTPases and is involved in organization of the actin cytoskeleton.[41] In addition, it is also crucial for neural crest development[42] and was identified as a putative PTF1α target in an acinar cell line.[23] An oncogenic role of Rhov is well documented in lung tumors.[43–45] A recent study has performed whole exon sequencing of 109 PDAC samples and found the genomic region of the Rhov gene (15q15.1) amplified in 2.8%.[46] However, a role of RHOV in PDAC initiation and maintenance is not reported so far. The extent to which upregulation of the class 5 P4-ATPase ATP10d[47] and the mitochondrial cytochrome C oxidase assembly factor Cox 18[48] have a functional role or, if applicable, a metabolic function during ADM or PanIN development is currently unknown. The same is true for PSAPL1, a protein of the prosaposin family. Interestingly, both factors, ATP10d and PSAPL1 seem to have a role in sphingolipid metabolism,[49] which was found to be altered in PDAC.[50] A correlation of Notch activity and CCNA1 expression was found in breast cancer patients.[51] Transcriptional de-repression of CCNA1 after loss of RBPJ is conceivable. However, indirect effects like proliferation of stroma cells could also be responsible for CCNA1 upregulation. Strikingly, however, all differentially expressed factors (Figure 7*F*) show no difference in expression during $Kras^{G12D}$-only mediated PanIN development (Supplementary Table 1).[24] This indeed suggests an effect of RBPJ loss on the differential expression of these factors.

RBPJ deficiency together with oncogenic KRAS expression markedly affects remodeling of the extracellular matrix in the pancreas (Figure 8*B*–*E*). Although there is no obvious tumorigenesis and inflammation, RBPJ loss is able to induce a massive chemokine/cytokine upregulation in the iKCR mice. Indeed, various family members of chemokine C-C motif and C-X-C motif ligands (Figure 8*D* and *E*, Supplementary Table 2) are already strongly elevated before any gross histological changes are evident. Cxcl2, Ccl28, Cxcl14, Ccl2, and Ccl7 showed the strongest differences compared with iKC mice and iKCR mice. CXCL2 recruits neutrophils in the early stage of tissue damage.[52] Interestingly, CCL28, CXCL14, and CCL20 are known to be elevated in the PDAC patients[53–55] and among those, CCL28 and CXCL14 correlate with a poor clinical outcome.[53,54] In contrast, CCL7 was considered to possess antitumoral effect in pancreatic cancer by enhancing natural killer cell infiltration.[56] Moreover, cytokines like IL-2, IL-6, IL-17a, and IL-11 were higher expressed in iKCR mice. IL-2 is one of the most well-known antitumorigenic acting cytokines by supporting cellular immunity. Interestingly, induced IL-2 expression, which is also overexpressed in pancreatitis patients, limited tumor growth and metastasis in pancreatic cancer by enhancing the expansion of cytotoxic T lymphocytes.[56,57] The IL-6 family includes IL-6 and IL-11, both support pancreatic tumorigenesis.[58,59] IL-17 produced by immune cells can induce PanIN development and progression[60] and might also be involved in stemness maintenance.[61]

Thus, RBPJ deficiency (or downregulation) in the context of oncogenic KRAS expression is able to (1) force PanIN development together with massive collagenic stroma formation, (2) promote *Notch1/Nrarp/Hes1* expression, and (3) remodel the extracellular matrix by upregulating a large number of chemokines, cytokines, mucin, and collagens.

lncRNAs Are Deregulated After RBPJ Depletion

An increasing number of studies highlight an important role of lncRNAs in tumorigenesis, including pancreatic cancer.[62] Our PCA analysis in terms of lncRNA expression (Figure 7*B*, Supplementary Table 3) suggest that RBPJ alone or in cooperation with PTF1α haploinsufficiency is involved the regulation of lncRNA expression. However, so far there

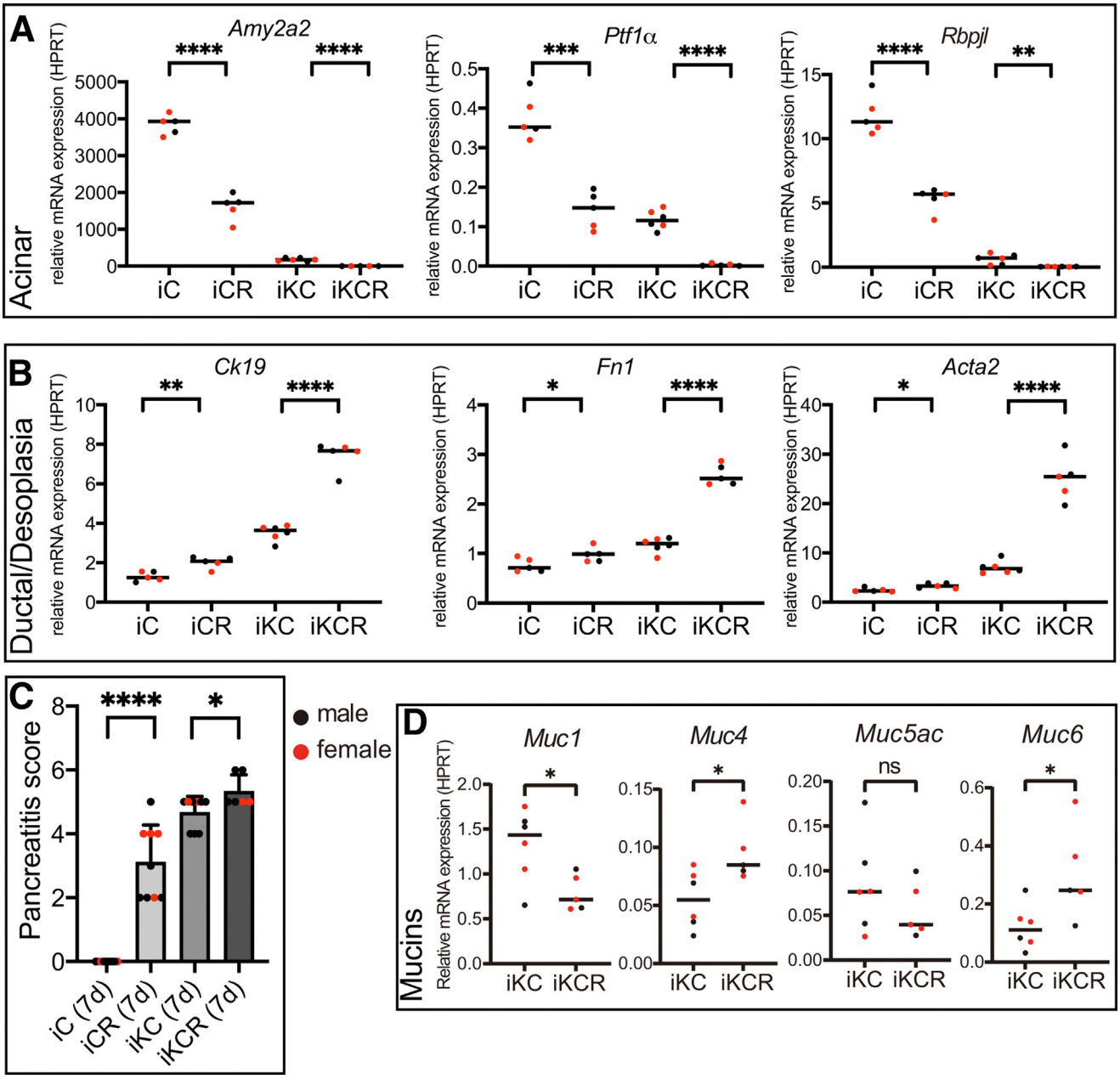

Figure 11. Real-time qPCR analysis of pancreata and pancreatitis scoring 7 days after the last cerulein treatment. RNA was extracted from iC (n = 5), iCR (n = 5), iKC (n = 6), and iKCR (n = 5) pancreata. The mRNA samples were analyzed for the expression of (*A*) acinar markers *Amy2a2*, *Ptf1α*, and *Rbpjl* and (*B*) ductal marker *Ck19* and fibrosis markers *Fn1* and *αSMA* (*Acta2*). (*C*) Pancreatitis scoring of iC, iCR, iKC, and iKCR mice 7 days after the last treatment with cerulein. (*D*) Real-time qPCR analysis for the expression of *Muc1*, *Muc4, Muc5ac*, and *Muc6.* Data were analyzed with an unpaired Student's *t* test in GraphPad Prism 5.0 and are presented as individual values as well as mean ± SEM. **P* < .1; ***P* < .01; ****P* < .001; *****P* < .0001. ns, not significant.

is lack of data about the role of PTF1α in lncRNA regulation. A few studies available suggest that specific lncRNAs are linked with RBPJ expression in colorectal cancer[63] and laryngeal carcinoma.[64] In addition, RBPJ can also regulate lncRNAs (ie, lncRNAs secreted due to RBPJ overexpression in macrophages limits progression of oral squamous cell carcinoma).[65] Furthermore, in glioblastoma cells, lncRNAs can be upregulated by the NICD/RBPJ/MAML2 axis.[66] Therefore, it is of great interest to identify pancreas-specific lncRNAs specifically regulated by RBPJ and/or PTF1α in the future.

Pancreatic Regeneration Is Delayed Upon RBPJ Deficiency

Notch signaling is vital for pancreatic regeneration after injury, and loss of Notch signaling significantly impairs

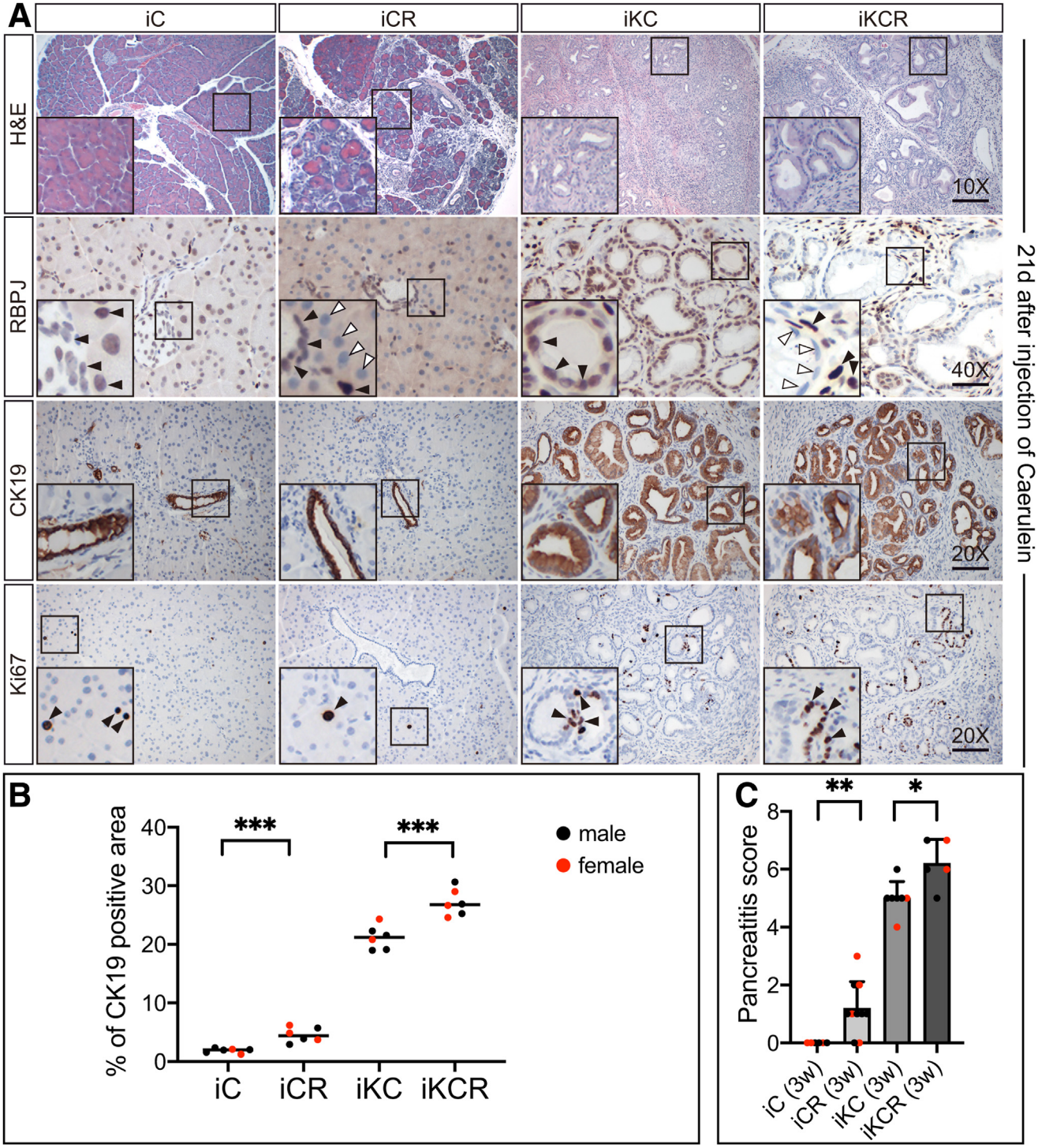

Figure 12. (Immuno)histological staining of pancreata from iC, iCR, iKC, and iKCR mice 21 days after cerulein-mediated induction of AP. (*A*) Representative images of pancreata from iC, iCR, iKC, and iKCR mice stained with hematoxylin and eosin (H&E) and IHC with antibodies against RBPJ, CK19, and Ki67. Magnifications of selected regions are shown in the left corner. Black and white arrows indicate RBPJ/Ki67-positive and RBPJ-negative cells, respectively. Scale bars represent 200 μm (10×), 100 μm (20×), and 50 μm (40×). (*B*) Quantification of CK19-positive area in pancreata from iC (n = 6), iCR (n = 6), iKC (n = 6), and iKCR (n = 5) mice. (*C*) Quantification of the pancreatitis score as described in the Materials and Methods 21 days after the last treatment with cerulein. Data were analyzed with an unpaired Student's *t* test in GraphPad Prism 5.0 and are presented as individual values as well as mean ± SEM. *, $P < .1$ **, $P < .01$; ***, $P < .001$.

regeneration after AP. Normally, acinar cells exposed to cerulein expresses higher levels of NOTCH1, NOTCH2, and HES1[27] and NOTCH1 deficiency was shown to impair their recovery after AP. In addition, embryonic deletion of *Hes1* in the exocrine pancreas impairs regeneration after AP.[29]

In this study, iCR mice underwent the inflammatory and early regeneration phase after AP induction with morphological alterations similar to iC mice (Figures 9*B* and 10). Thus, RBPJ does not have an instructive role in these phases. Importantly, the pancreatic refinement as the last phase of regeneration after AP was significantly delayed in iCR mice. Even 21 days after cerulein treatment, necrotizing regions were not yet fully resolved (Figure 12). After 2 months, however, the iCR pancreas was fully recovered.

Pancreatic regeneration is impaired in the iCR mouse model (Figures 10, 11, and 12). We suggest that lack of the PTF1α-RBPJ complex during the redifferentiation of acinar cells limits RBPJL induction and thereby delays the final steps of acinar regeneration including terminal differentiation. Because the deletion efficiency of RBPJ did not reach 100%, we cannot exclude that RBPJL might be produced at low levels and thus available for autoactivation of the PTF1α-RBPJL complex. Also, RBPJL might be activated by yet unknown factors/regulators independent of RBPJ and/or PTF1α. Therefore, a conditional RBPJL knockout mouse model might be helpful for future studies to test whether RBPJL is involved in maintenance and homeostasis of acinar cells as well as their regeneration after AP.

In conclusion, RBPJ deficiency impairs pancreatic regeneration, probably through limiting RBPJL expression.

Pancreatic Regeneration Is Impaired Upon RBPJ Deficiency in the Context of KRAS^{G12D} Expression

Pancreatic regeneration is usually fully blocked by oncogenic KRAS expression characterized by upregulation of *Hes1* in ADM and PanIN lesions. Interestingly, ADM lesions without *Hes1* expression can be differentiated back to acinar cells even with the induction of mutated Kras,[36] further suggesting that HES1 promotes pancreatic transformation. In iKCR mice, *Hes1* expression was remarkably increased even before AP challenge (Figure 8*A*). Therefore, cerulein treated iKCR mice are presumed to show accelerated pancreatic desmoplasia.

Indeed, already 1 day after exposure to cerulein, tissue damage was more severe in iKCR mice exhibiting RBPJ deletion compared with iKC mice (Figure 9*B* and *D*). Desmoplasia occurred and persisted in both iKCR mice and iKC mice (Figures 10, 11, and 12). At the same time, less severely damaged pancreata in iKC mice were consistent with higher levels of acinar marker and lower levels of ductal/desmoplasia marker compared with iKCR mice (Figure 11*A* and *B*). Interestingly, cerulein-treated iKC and iKCR pancreata presented different subcellular mucin expression pattern with a mixed mucin phenotype in iKC mice compared with a predominant cytoplasmic expression in iKCR mice (Figures 10 and 11*D*). *Muc4* and *Muc6* expression was increased in iKCR mice compared with iKC mice, while *Muc1* and *Muc5ac* were less expressed. Because these mucins are known to be involved in the PanIN/PDAC development,[67–71] a more detailed evaluation of the specific mucin phenotype in iKCR and iKC is required to define the specific role of RBPJ.

Taken together, we identified a prominent downregulation or loss of RBPJ expression in human PDAC specimen. When we recapitulate this issue in corresponding mouse models, RBPJ deficiency in the context of KRAS^{G12D} expression was found to facilitate pancreatic acinar cell transformation together with marked remodeling of the extracellular matrix. Therefore, we suggest, that RBPJ function is critically involved in cell-autonomous and non–cell-autonomous mechanisms protecting pancreatic acinar cells from KRAS-mediated PanIN initiation and progression.

Materials and Methods

All authors had access to the study data and had reviewed and approved the final manuscript.

Human Histological Specimens and IHC Analysis

Three commercially available tissue microarrays (US Biomax; HPan-Ade120Su-01 [63 cases], HPan-Ade170Su-01 [99 cases], HPan-A150CS-02 [78 cases]) were subjected to immunohistochemistry with an anti-RBPJ antibody (7A11; kindly provided by Prof. Kempkes, München). RBPJ immunostaining was evaluated on a Motic BA410 microscope (Motic Images Plus 2.0 software) and overall RBPJ expression level was staged (null, low, medium, high).

Mice

All animal procedures were performed according to protocols approved by the Baden-Württemberg Animal Committee (TVA-1410). *Rbpj*$^{flox/flox}$ mice,[21] *Ptf1α-Cre*$^{ERT/+}$ mice (referred to as iC mice),[22] and *LSL-Kras*$^{G12D/+}$ mice[72] were maintained on a C57BL/6 background and intercrossed to generate *Ptf1α-Cre*^{ERT};*Rbpj*$^{flox/flox}$ mice (referred to as iCR mice) and *Ptf1α-Cre*$^{ERT/+}$;*LSL-Kras*$^{G12D/+}$;*Rbpj*$^{flox/flox}$ mice (referred to as iKCR mice).

RBPJ deletion was induced by activation of the Cre recombinase. Therefore, 6- to 8-week-old mice were administered TAM (intraperitoneal, 5 mg/200 μL; Merck; #T5648; dissolved in ClinOleic 20% [Baxter]) on 5 consecutive days. Littermate control mice were injected with 200 μL ClinOleic 20%. Mice were carefully monitored and pancreata were harvested at the indicated time points.

Polymerase Chain Reaction

DNA isolated from mouse ear biopsy was analyzed by genotyping PCR using primers (Table 1) specific for the *Cre*^{ERTM}, *Rbpj*^{wt}, *Rbpj*^{flox}, and *LSL-Kras*^{G12D} allele. DNA isolated from iCR mouse pancreata was analyzed by deletion PCR using primers (Table 1) specific for the *Rbpj*^{del} and *Rbpj*^{flox} allele. PCR products were separated on 1.5% agarose gels.

Tissue Processing and IHC Staining

Formalin-fixed, paraffin-embedded mouse pancreata were dissected into 4-mm-thin sections, deparaffinized, and

Table 1. Primers Used for Genotyping and Deletion Polymerase Chain Reaction Analyses

Name	Primer Sequence
Cre^{ERTM}_F	5′-AACCTGGATAGTGAAACAGGGGC-3′
Cre^{ERTM}_R	5′-TTCCATGGAGCGAACGACGAGACC-3′
*rbpj*_wt_F	5′-GTTCTTAACCTGTTGGTCGGAACC-3′
*rbpj*_wt_R	5′-GCTTGAGGCTTGATGTTCTGTATTGC-3′
*rbpj*_flox_F	5′-GAAGGTCGGTTGACACCAGATAGC-3′
*rbpj*_flox_R	5′-GCAATCCATCTTGTTCAATGGCC-3′
*rbpj*_del_F	5′-GACCTTGGTTTGTTGTTTGGGTT-3′
*rbpj*_del_R	5′-GAGAGACAAGCCTAGAACAGG-3′
LSL-$Kras^{G12D}$_F	5′-AGCTAGCCACCATGGCTTGAGTAAGTCTGCA-3′
LSL-$Kras^{G12D}$_R	5′-CCTTTACAAGCGCACGCAGACTGTAGA-3′

rehydrated. After blocking endogenous peroxidases with 3% hydrogen peroxide (Merck; #1.07209.0250), microwave antigen retrieval (unmasking solution; Vector; #H-3300), and blocking (2% bovine serum albumin [BSA] in Tris-buffered saline [TBS] and avidin/biotin blocking kit; Vector; #SP-2001), primary antibodies (Table 2) diluted in 2% BSA (in TBS) were applied and incubated overnight at 4°C in a humidified chamber. The next day, sections were washed and incubated with the biotin-conjugated secondary antibodies diluted in 2% BSA in TBS for 30 minutes at room temperature. When using mouse antibodies, the M.O.M. blocking kit (Vector; #BMK2202) was applied following the manufacturer's instructions. Briefly, the primary antibody was applied for 1 hour at room temperature with biotinylated secondary antibodies (Table 3) added for 10 minutes at room temperature. Visualization of antibody binding was achieved with the Vectastain Elite ABC reagents (Vector; #PK-6100) and NovaRed (Vector; #SK-4800) according to the manufacturer's instructions. The sections were counterstained with 20% hematoxylin and eosin.

For Alcian blue staining, deparaffinized and rehydrated sections were incubated in 1% Alcian blue solution (pH 2.5; Biognost; #AB2-OT-1L) for up to 30 minutes at room temperature prior to counterstaining with nuclear fast red (Vector; #H-3403).

For Sirius red staining, deparaffinized and rehydrated sections were stained in Weigert's hematoxylin (Roth; #X907.1) for 8 minutes, washed, and incubated in the Picrosirius red solution (0.5 g Direct Red 80 [Merck; #365548] in 50 mL saturated aqueous solution of picric acid [Merck; #P6744]) for 1 hour before sections were washed with acidified water (5 mL acetic acid glacial [VWR; #20104.298] in 1 L distilled water).

Histological images were acquired with a Motic BA410 microscope and Motic Images Plus 2.0 software.

Quantification of Pancreatic Lesions

Quantification of ADM/PanIN events was performed with FIJI software (https://imagej.net/software/fiji/) trained with the IHC tool (https://imagej.nih.gov/ij/plugins/ihc-toolbox/index.html). At least 10 randomly selected fields were photographed at 20× magnification, and the percentage of the positively stained area was scored. Blind grading and quantification of ADM and PanIN lesions by a second examiner were carried out on at least 40 randomly selected fields per group and time point (photographed at 20× magnification), from histological hematoxylin and eosin sections of all animals enrolled in the study (n = 6 animals per group and time point). PanINs were scored according to the human PanIN classification system,[73–75] from PanIN-1 (low-grade dysplasia) to PanIN-3 (high-grade dysplasia). Each lesion was graded based on its highest-grade component.

Isolation of Primary Pancreatic Acinar Cells and ADM Assay

Freshly isolated pancreata were rinsed twice in ice cold Hank's Balanced Salt Solution (HBSS) (Corning; #21-021-CV) and centrifuged at 1000 rpm for 3 minutes at 4 °C. The pancreas was then sliced into 1- to 5-mm pieces, and digested with 10 mL collagenase P solution (2 mg; Roche; #11213857001) for 20–30 minutes at 37°C. Mechanical dissociation was performed by up and down pipetting of the cells (10 mL pipette) every 5 minutes. To stop the digestion, 10 mL ice cold washing solution (HBSS with 5% heat-inactivated fetal calf serum [FCS] and 10 mM HEPES [Gibco #15630-056]) was applied. After centrifugation (1000 rpm for 2 minutes at 4°C) and washing twice with washing solution, the mixture was filtered through a 100-μm cell strainer (Corning; #431752). Afterward, the cell suspension was added dropwise on top of 2 mL HBSS solution supplemented with 30% FCS. After centrifugation at 1000 rpm for 2 minutes at 4°C, the acinar cells were washed

Table 2. Primary Antibody Used in Immunohistochemistry

Antibody	Dilution	Species	Company	Cat. No.
Anti-Amylase (polyclonal IgG)	1:100	Rabbit	Merck	A8273
Anti-αSMA (polyclonal IgG)	1:200	Rabbit	Abcam	ab5694
Anti-CK19 (monoclonal IgG)	1:100	Rat	DSHB	TROMA-III
Anti-Insulin (monoclonal IgG)	1:800	Mouse	Cell signaling	8138S
Anti-Ki67 (monoclonal IgG)	1:200	Rabbit	Invitrogen	MA5-14520
Anti-PTF1α (monoclonal IgG)	1:500	Mouse	BD Pharmingen	564745
Anti-RBPJ (monoclonal IgG)	1:100	Rat	Provided by Prof. Kempkes, Munich	7A11

Table 3. Secondary Antibody Used in Immunohistochemistry

Antibody	Dilution	Company	Cat. No
Rabbit Anti-Rat IgG Antibody, mouse adsorbed (H+L), Biotinylated	1:100	Vector	BA-4001
Goat Anti-Rabbit IgG Antibody (H+L), Biotinylated	1:100	Vector	BA-1000
M.O.M. (Mouse on Mouse) Elite Immunodetection Kit, Peroxidase	1:250	Vector	PK-2200

with 10 mL Waymouth's medium (Gibco; #31220-023; supplemented with 1% FCS, 0.1 mg/mL trypsin inhibitor [Merck; #T9003] and 1 μg/mL dexamethasone [Merck; #D2915]). Finally, acinar cells were mixed with Waymouth's medium and growth factor–reduced Matrigel (at a ratio 1:1.5; Corning; #354230) and seeded on 24-well plates. Each well was incubated with 400 μL of the cell-gel mixture for 30 minutes at 37°C. Subsequently, 600 μL of medium was applied to each well. Transforming growth factor α (TGFα, 500 ng/well; Merck; #T7924) was added as the positive control. The images were acquired using a Leica LEITZ DM-IRBE microscope and processed by QCapture Suite PLUS software (QImaging).

RNA Extraction, Complementary DNA Synthesis, and qPCR Analyses

Total RNA was extracted from pancreas tissue using the QIAzol Lysis Reagent (Qiagen; #79306) and purified using the RNeasy Mini Kit (Qiagen; #74106). Total RNA from

Table 4. Primers Used for Quantitative Polymerase Chain Reaction Analyses

Gene	Assay (Qiagen)	ID No.
9430085M18Rik, mouse	RT^2 lncRNA qPCR Assay for Mouse 9430085M18Rik	LPM07692A
Actin, mouse	Mm_Actb_2_SG QuantiTect Primer Assay	QT01136772
Amylase, mouse	Mm_Amy2a2_1_SG QuantiTect Primer Assay	QT02276351
Atp10d, mouse	Mm_Atp10d_2_SG QuantiTect Primer Assay	QT01063685
Bhlha 15, mouse	Mm_Bhlha15_1_SG QuantiTect Primer Assay	QT00315182
Ccna1, mouse	Mm_Ccna1_1_SG QuantiTect Primer Assay	QT00493255
Cela, mouse	Mm_Cela1_1_SG QuantiTect Primer Assay	QT00100226
Ck19, mouse	Mm_Krt19_1_SG QuantiTect Primer Assay	QT00156667
Cox18, mouse	Mm_Cox18_2_SG QuantiTect Primer Assay	QT00301399
Ctrb1, mouse	Mm_Ctrb1_1_SG QuantiTect Primer Assay	QT00122066
Cpa1, mouse	Mm_Cpa1_1_SG QuantiTect Primer Assay	QT00251930
Hprt, mouse	Mm_Hprt_1_SG QuantiTect Primer Assay	QT00166768
Muc1, mouse	Mm_Muc1_1_SG QuantiTect Primer Assay	QT00105784
Muc4, mouse	Mm_Muc4_2_SG QuantiTect Primer Assay	QT00138663
Muc5ac, mouse	Mm_Muc5ac_va.1_SG QuantiTect Primer Assay	QT01161111
Muc6, mouse	Mm_Muc6_1_SG QuantiTect Primer Assay	QT00151627
Fn1, mouse	Mm_Fn1_1_SG QuantiTect Primer Assay	QT00135758
a-SMA, *mouse*	Mm_Acta2_1_SG QuantiTect Primer Assay	QT00140119
Notch1, mouse	Mm_Notch1_1_SG QuantiTect Primer Assay	QT00156982
Rbpj, mouse	Mm_Rbpj_1_SG QuantiTect Primer Assay	QT00075607
Rbpjl, mouse	Mm_Rbpjl_1_SG QuantiTect Primer Assay	QT00129416
Rhov, mouse	Mm_Rhov_2_SG QuantiTect Primer Assay	QT02300291
Pnlip, mouse	Mm_Pnlip_1_SG QuantiTect Primer Assay	QT00117740
Psap1, mouse	Mm_Psap_1_SG QuantiTect Primer Assay	QT00162953
Ptf1α, mouse	Mm_Ptf1a_1_SG QuantiTect Primer Assay	QT00124187
Hes1, mouse	Mm_Hes1_1_SG QuantiTect Primer Assay	QT00313537
Insulin, mouse	Mm_Ins1_2_SG QuantiTect Primer Assay	QT01660855
Gata6, mouse	Mm_Gata6_1_SG QuantiTect Primer Assay	QT00171297
Gkn1, mouse	Mm_Gkn1_1_SG QuantiTect Primer Assay	QT00125636
Glucagon, mouse	Mm_Gcg_1_SG QuantiTect Primer Assay	QT00124033
Nrarp, mouse	Mm_Nrarp_1_SG QuantiTect Primer Assay	QT00262199
Nr5a2, mouse	Mm_Nr5a2_1_SG QuantiTect Primer Assay	QT00106778

isolated acinar cells was purified using the QIAshredder (Qiagen; #79656) and RNeasy Micro Kit (Qiagen; #74004). All RNA isolations were performed according to manufacturer's instructions and included DNase I treatment (Qiagen; #79254). RNA concentration was determined with the NanoDrop 2000 (PeqLab Biotechnology) and RNA converted to complementary DNA with SuperScript II reverse transcriptase (Invitrogen; #18064-014). QuantiTect SYBR Green PCR kit (Qiagen; #204056) was used for the qPCR reaction on a Light Cycler 480 Real-Time PCR system device (Roche). The specific mRNA expression of the genes of interest was calculated using the ΔΔCt method and normalized to the housekeeping gene β-actin (Qiagen; #QT01136772). The primers used for qPCR analyses are listed in Table 4.

Statistical Analysis

Statistical tests and graphical data presentations were performed by the means of GraphPad Prism 5.0 software (GraphPad Software). The statistical significance of differences between the indicated groups was tested by unpaired Student's t test. All data represent the mean ± SD. In addition, comparison of overall survival was analyzed by the GraphPad Prism log-rank (Mantel-Cox) test. The level of statistical significance is presented by asterisks (*) with P values $>.05$ (not significant), $\leq.05$ (*), $\leq.01$ (**), $\leq.001$ (***), and $\leq.0001$ (****).

RNA Sequencing

Raw RNA-seq were mapped to the mouse reference genome GRCm38 using HISAT2.[76–79] RNA-seq mapping QC was performed using Picard tools (https://broadinstitute.github.io/picard/). The gene expression count matrix was generated using featureCounts.[80] Downstream analyses including clustering, heatmaps, PCA, and self-organizing map were conducted using R and Bioconductor packages.[81–83] Data for the heatmap and Venn diagram are shown in Supplementary Table 1. Gene set enrichment analysis (GSEA) was performed using the standalone java implementation of the package.[84,85] Data for GSEA data are shown in Supplementary Table 2. Raw reads and count matrix have been uploaded to Gene Expression Omnibus, accession number GSE189756.

Cerulein-Induced AP

The application of cerulein (Merck; #C9026) is the commonly used method for induction of AP in mice. Four weeks after TAM injection, the mice were injected (intraperitoneally) 8 times on 2 consecutive days with an appropriate dose of cerulein (50 μg/kg dissolved in phosphate-buffered saline). The injection volume depended on the initial weight of the animals. The control groups received a volume-adjusted administration of the vehicle phosphate-buffered saline in the same injection interval. Animals were killed painlessly after the given time periods. During the subsequent necropsy, pancreata were collected for mRNA extraction and histological analysis. Pancreatitis score was established as previously described[86] scoring edema, inflammation, and necrosis in a blinded fashion on duplicate hematoxylin and eosin–stained section from at least 6 mice per genotype and time point.

Data Transparency

Raw reads and count matix of RNA-sequencing data are available at the Gene Expression Omnibus under accession number GSE189756. In this study, downstream analyses and GSEA were used as indicated in the Materials and Methods. All other data (additional raw data and independent replicates) supporting the study findings are available upon requesting from the corresponding author.

Supplementary Material

Supplementary data to this article can be found online at https://doi.org/10.1016/j.jcmgh.2023.07.013.

References

1. Ryan DP, Hong TS, Bardeesy N. Pancreatic adenocarcinoma. N Engl J Med 2014;371:2140–2141.
2. Alexandrov LB, Nik-Zainal S, Wedge DC, et al. Signatures of mutational processes in human cancer. Nature 2013;500:415–421.
3. Habbe N, Shi G, Meguid RA, et al. Spontaneous induction of murine pancreatic intraepithelial neoplasia (mPanIN) by acinar cell targeting of oncogenic Kras in adult mice. Proc Natl Acad Sci U S A 2008;105:18913–18918.
4. Miyamoto Y, Maitra A, Ghosh B, et al. Notch mediates TGF alpha-induced changes in epithelial differentiation during pancreatic tumorigenesis. Cancer Cell 2003;3:565–576.
5. Monastirioti M, Giagtzoglou N, Koumbanakis KA, et al. Drosophila Hey is a target of Notch in asymmetric divisions during embryonic and larval neurogenesis. Development 2010;137:191–201.
6. Katoh M. Networking of WNT, FGF, Notch, BMP, and Hedgehog signaling pathways during carcinogenesis. Stem Cell Rev 2007;3:30–38.
7. Hingorani SR, Petricoin EF, Maitra A, et al. Preinvasive and invasive ductal pancreatic cancer and its early detection in the mouse. Cancer Cell 2003;4:437–450.
8. Thomas MM, Zhang Y, Mathew E, et al. Epithelial Notch signaling is a limiting step for pancreatic carcinogenesis. BMC Cancer 2014;14:862.
9. Plentz R, Park JS, Rhim AD, et al. Inhibition of gamma-secretase activity inhibits tumor progression in a mouse model of pancreatic ductal adenocarcinoma. Gastroenterology 2009;136:1741–1749.e6.
10. Abel EV, Kim EJ, Wu J, et al. The Notch pathway is important in maintaining the cancer stem cell population in pancreatic cancer. PLoS One 2014;9:e91983.
11. Hanlon L, Avila JL, Demarest RM, et al. Notch1 functions as a tumor suppressor in a model of K-ras-induced pancreatic ductal adenocarcinoma. Cancer Res 2010;70:4280–4286.
12. Avila JL, Kissil JL. Notch signaling in pancreatic cancer: oncogene or tumor suppressor? Trends Mol Med 2013;19:320–327.

13. Mazur PK, Einwachter H, Lee M, et al. Notch2 is required for progression of pancreatic intraepithelial neoplasia and development of pancreatic ductal adenocarcinoma. Proc Natl Acad Sci U S A 2010;107:13438–13443.
14. Borggrefe T, Oswald F. The Notch signaling pathway: transcriptional regulation at Notch target genes. Cell Mol Life Sci 2009;66:1631–1646.
15. Masui T, Long Q, Beres TM, et al. Early pancreatic development requires the vertebrate Suppressor of Hairless (RBPJ) in the PTF1 bHLH complex. Genes Dev 2007;21:2629–2643.
16. Masui T, Swift GH, Deering T, et al. Replacement of Rbpj with Rbpjl in the PTF1 complex controls the final maturation of pancreatic acinar cells. Gastroenterology 2010; 139:270–280.
17. Cras-Meneur C, Conlon M, Zhang Y, et al. Early pancreatic islet fate and maturation is controlled through RBP-Jkappa. Sci Rep 2016;6:26874.
18. Oka C, Nakano T, Wakeham A, et al. Disruption of the mouse RBP-J kappa gene results in early embryonic death. Development 1995;121:3291–3301.
19. Nakhai H, Siveke JT, Klein B, et al. Conditional ablation of Notch signaling in pancreatic development. Development 2008;135:2757–2765.
20. Kulic I, Robertson G, Chang L, et al. Loss of the Notch effector RBPJ promotes tumorigenesis. J Exp Med 2015; 212:37–52.
21. Han H, Tanigaki K, Yamamoto N, et al. Inducible gene knockout of transcription factor recombination signal binding protein-J reveals its essential role in T versus B lineage decision. Int Immunol 2002;14:637–645.
22. Kopinke D, Brailsford M, Pan FC, et al. Ongoing Notch signaling maintains phenotypic fidelity in the adult exocrine pancreas. Dev Biol 2012;362:57–64.
23. Thompson N, Gesina E, Scheinert P, et al. RNA profiling and chromatin immunoprecipitation-sequencing reveal that PTF1a stabilizes pancreas progenitor identity via the control of MNX1/HLXB9 and a network of other transcription factors. Mol Cell Biol 2012;32:1189–1199.
24. Paul MC, Schneeweis C, Falcomata C, et al. Non-canonical functions of SNAIL drive context-specific cancer progression. Nat Commun 2023;14:1201.
25. Liou GY, Bastea L, Fleming A, et al. The presence of interleukin-13 at pancreatic ADM/PanIN lesions alters macrophage populations and mediates pancreatic tumorigenesis. Cell Rep 2017;19:1322–1333.
26. Bazzichetto C, Conciatori F, Luchini C, et al. From genetic alterations to tumor microenvironment: the Ariadne's string in pancreatic cancer. Cells 2020;9:309.
27. Siveke JT, Lubeseder-Martellato C, Lee M, et al. Notch signaling is required for exocrine regeneration after acute pancreatitis. Gastroenterology 2008;134:544–555.
28. Carrière C, Young AL, Gunn JR, et al. Acute pancreatitis markedly accelerates pancreatic cancer progression in mice expressing oncogenic Kras. Biochem Biophys Res Commun 2009;382:561–565.
29. Kong B, Bruns P, Behler NA, et al. Dynamic landscape of pancreatic carcinogenesis reveals early molecular networks of malignancy. Gut 2018;67:146–156.
30. Beres TM, Masui T, Swift GH, et al. PTF1 is an organ-specific and Notch-independent basic helix-loop-helix complex containing the mammalian Suppressor of Hairless (RBP-J) or its paralogue, RBP-L. Mol Cell Biol 2006;26:117–130.
31. Krah NM, De La OJ, Swift GH, et al. The acinar differentiation determinant PTF1A inhibits initiation of pancreatic ductal adenocarcinoma. Elife 2015;4:e07125.
32. Sakikubo M, Furuyama K, Horiguchi M, et al. Ptf1a inactivation in adult pancreatic acinar cells causes apoptosis through activation of the endoplasmic reticulum stress pathway. Sci Rep 2018;8:15812.
33. von Figura G, Morris JP 4th, Wright CVE, et al. Nr5a2 maintains acinar cell differentiation and constrains oncogenic Kras-mediated pancreatic neoplastic initiation. Gut 2014;63:656–664.
34. Pin CL, Rukstalis JM, Johnson C, et al. The bHLH transcription factor Mist1 is required to maintain exocrine pancreas cell organization and acinar cell identity. J Cell Biol 2001;155:519–530.
35. Direnzo D, Hess DA, Damsz B, et al. Induced Mist1 expression promotes remodeling of mouse pancreatic acinar cells. Gastroenterology 2012;143:469–480.
36. Nishikawa Y, Kodama Y, Shiokawa M, et al. Hes1 plays an essential role in Kras-driven pancreatic tumorigenesis. Oncogene 2019;38:4283–4296.
37. Waters AM, Der CJ. KRAS: The critical driver and therapeutic target for pancreatic cancer. Cold Spring Harb Perspect Med 2018;8:a031435.
38. De La OJ, Emerson LL, Goodman JL, et al. Notch and Kras reprogram pancreatic acinar cells to ductal intraepithelial neoplasia. Proc Natl Acad Sci U S A 2008; 105:18907–18912.
39. Hruban RH, Adsay NV, Albores-Saavedra J, et al. Pathology of genetically engineered mouse models of pancreatic exocrine cancer: consensus report and recommendations. Cancer Res 2006;66:95–106.
40. Avila JL, Troutman S, Durham A, et al. Notch1 is not required for acinar-to-ductal metaplasia in a model of Kras-induced pancreatic ductal adenocarcinoma. PLoS One 2012;7:e52133.
41. Aronheim A, Broder YC, Cohen A, et al. Chp, a homologue of the GTPase Cdc42Hs, activates the JNK pathway and is implicated in reorganizing the actin cytoskeleton. Curr Biol 1998;8:1125–1128.
42. Faure S, Fort P. Atypical RhoV and RhoU GTPases control development of the neural crest. Small GTPases 2015;6:174–177.
43. Zhang D, Jiang Q, Ge X, et al. RHOV promotes lung adenocarcinoma cell growth and metastasis through JNK/c-Jun pathway. Int J Biol Sci 2021;17:2622–2632.
44. Jin ML, Gong Y, Ji P, et al. In vivo CRISPR screens identify RhoV as a pro-metastasis factor of triple-negative breast cancer. Cancer Sci 2023;114:2375–2385.
45. Chen H, Xia R, Jiang L, et al. Overexpression of RhoV promotes the progression and EGFR-TKI resistance of lung adenocarcinoma. Front Oncol 2021;11:619013.
46. Witkiewicz AK, McMillan EA, Balaji U, et al. Whole-exome sequencing of pancreatic cancer defines genetic diversity and therapeutic targets. Nat Commun 2015;6:6744.

47. Andersen JP, Vestergaard AL, Mikkelsen SA, et al. P4-ATPases as phospholipid flippases-structure, function, and enigmas. Front Physiol 2016;7:275.
48. Bourens M, Barrientos A. Human mitochondrial cytochrome c oxidase assembly factor COX18 acts transiently as a membrane insertase within the subunit 2 maturation module. J Biol Chem 2017;292:7774–7783.
49. Hymel E, Fisher KW, Farazi PA. Differential methylation patterns in lean and obese non-alcoholic steatohepatitis-associated hepatocellular carcinoma. BMC Cancer 2022; 22:1276.
50. Rozeveld CN, Johnson KM, Zhang L, et al. KRAS controls pancreatic cancer cell lipid metabolism and invasive potential through the lipase HSL. Cancer Res 2020; 80:4932–4945.
51. Chen YL, Lee KT, Wang CY, et al. Low expression of cytosolic NOTCH1 predicts poor prognosis of breast cancer patients. Am J Cancer Res 2022;12:2084–2101.
52. Panahi Y, Fakhari S, Mohammadi M, et al. Glycyrrhizin down-regulates CCL2 and CXCL2 expression in cerulein-stimulated pancreatic acinar cells. Am J Clin Exp Immunol 2015;4:1–6.
53. Yan J, Yuan P, Gui L, et al. CCL28 downregulation attenuates pancreatic cancer progression through tumor cell-intrinsic and -extrinsic mechanisms. Technol Cancer Res Treat 2021;20:15330338211068958.
54. Wente MN, Mayer C, Gaida MM, et al. CXCL14 expression and potential function in pancreatic cancer. Cancer Lett 2008;259:209–217.
55. Rubie C, Frick VO, Ghadjar P, et al. CCL20/CCR6 expression profile in pancreatic cancer. J Transl Med 2010;8:45.
56. Dempe S, Lavie M, Struyf S, et al. Antitumoral activity of parvovirus-mediated IL-2 and MCP-3/CCL7 delivery into human pancreatic cancer: implication of leucocyte recruitment. Cancer Immunol Immunother 2012; 61:2113–2123.
57. Wagner K, Schulz P, Scholz A, et al. The targeted immunocytokine L19-IL2 efficiently inhibits the growth of orthotopic pancreatic cancer. Clin Cancer Res 2008; 14:4951–4960.
58. Lesina M, Kurkowski MU, Ludes K, et al. Stat3/Socs3 activation by IL-6 transsignaling promotes progression of pancreatic intraepithelial neoplasia and development of pancreatic cancer. Cancer Cell 2011;19:456–469.
59. Shin SY, Choi C, Lee HG, et al. Transcriptional regulation of the interleukin-11 gene by oncogenic Ras. Carcinogenesis 2012;33:2467–2476.
60. McAllister F, Bailey JM, Alsina J, et al. Oncogenic Kras activates a hematopoietic-to-epithelial IL-17 signaling axis in preinvasive pancreatic neoplasia. Cancer Cell 2014;25:621–637.
61. Zhang Y, Zoltan M, Riquelme E, et al. Immune cell production of interleukin 17 induces stem cell features of pancreatic intraepithelial neoplasia cells. Gastroenterology 2018;155:210–223.e3.
62. Reese M, Dhayat SA. Small extracellular vesicle non-coding RNAs in pancreatic cancer: molecular mechanisms and clinical implications. J Hematol Oncol 2021;14:141.
63. Chen GQ, Liao ZM, Liu J, et al. lncRNA FTX promotes colorectal cancer cells migration and invasion by miRNA-590-5p/RBPJ axis. Biochem Genet 2021; 59:560–573.
64. Yuan Z, Xiu C, Song K, et al. Long non-coding RNA AFAP1-AS1/miR-320a/RBPJ axis regulates laryngeal carcinoma cell stemness and chemoresistance. J Cell Mol Med 2018;22:4253–4262.
65. Ai Y, Wei H, Wu S, et al. Exosomal lncRNA LBX1-AS1 derived from RBPJ overexpressed-macrophages inhibits oral squamous cell carcinoma progress via miR-182-5p/FOXO3. Front Oncol 2021;11:605884.
66. Wu J, Wang N, Yang Y, et al. LINC01152 upregulates MAML2 expression to modulate the progression of glioblastoma multiforme via Notch signaling pathway. Cell Death Dis 2021;12:115.
67. Matsuyama M, Kondo F, Ishihara T, et al. Evaluation of pancreatic intraepithelial neoplasia and mucin expression in normal pancreata. J Hepatobiliary Pancreat Sci 2012;19:242–248.
68. Pai P, Rachagani S, Lakshmanan I, et al. The canonical Wnt pathway regulates the metastasis-promoting mucin MUC4 in pancreatic ductal adenocarcinoma. Mol Oncol 2016;10:224–239.
69. Lo ST, Pantazopouos P, Medarova Z, et al. Presentation of underglycosylated mucin 1 in pancreatic adenocarcinoma (PDAC) at early stages. Am J Cancer Res 2016;6:1986–1995.
70. Sierzega M, Młynarski D, Tomaszewska R, et al. Semiquantitative immunohistochemistry for mucin (MUC1, MUC2, MUC3, MUC4, MUC5AC, and MUC6) profiling of pancreatic ductal cell adenocarcinoma improves diagnostic and prognostic performance. Histopathology 2016;69:582–591.
71. Thompson CM, Cannon A, West S, et al. Mucin expression and splicing determine novel subtypes and patient mortality in pancreatic ductal adenocarcinoma. Clin Cancer Res 2021;27:6787–6799.
72. Jackson EL, Willis N, Mercer K, et al. Analysis of lung tumor initiation and progression using conditional expression of oncogenic K-ras. Genes Dev 2001;15:3243–3248.
73. Klein WM, Hruban RH, Klein-Szanto AJ, et al. Direct correlation between proliferative activity and dysplasia in pancreatic intraepithelial neoplasia (PanIN): additional evidence for a recently proposed model of progression. Mod Pathol 2002;15:441–447.
74. Hruban RH, Maitra A, Goggins M. Update on pancreatic intraepithelial neoplasia. Int J Clin Exp Pathol 2008; 1:306–316.
75. Cornish TC, Hruban RH. Pancreatic intraepithelial neoplasia. Surg Pathol Clin 2011;4:523–535.
76. Zhang Y, Park C, Bennett C, et al. Rapid and accurate alignment of nucleotide conversion sequencing reads with HISAT-3N. Genome Res 2021;31:1290–1295.
77. Kim D, Paggi JM, Park C, et al. Graph-based genome alignment and genotyping with HISAT2 and HISAT-genotype. Nat Biotechnol 2019;37:907–915.
78. Kim D, Langmead B, Salzberg SL. HISAT: a fast spliced aligner with low memory requirements. Nat Methods 2015;12:357–360.
79. Pertea M, Kim D, Pertea GM, et al. Transcript-level expression analysis of RNA-seq experiments with HISAT, StringTie and Ballgown. Nat Protoc 2016;11:1650–1667.

80. Liao Y, Smyth GK, Shi W. featureCounts: an efficient general purpose program for assigning sequence reads to genomic features. Bioinformatics 2014; 30:923–930.
81. Gentleman R, Carey V. Visualization and annotation of genomic experiments. In: Parmigiani G, Garrett ES, Irizarry RA, et al., editors. The Analysis of Gene Expression Data: Methods and Software. New York, NY: Springer; 2003:46–72.
82. Huber W, Carey VJ, Gentleman R, et al. Orchestrating high-throughput genomic analysis with Bioconductor. Nat Methods 2015;12:115–121.
83. Gentleman RC, Carey VJ, Bates DM, et al. Bioconductor: open software development for computational biology and bioinformatics. Genome Biol 2004; 5:R80.
84. Subramanian A, Tamayo P, Mootha VK, et al. Gene set enrichment analysis: a knowledge-based approach for interpreting genome-wide expression profiles. Proc Natl Acad Sci U S A 2005;102:15545–15550.
85. Mootha VK, Lindgren CM, Eriksson KF, et al. PGC-1alpha-responsive genes involved in oxidative phosphorylation are coordinately downregulated in human diabetes. Nat Genet 2003;34:267–273.
86. Van Laethem JL, Eskinazi R, Louis H, et al. Multisystemic production of interleukin 10 limits the severity of acute pancreatitis in mice. Gut 1998;43:408–413.

Received March 23, 2022. Accepted July 28, 2023.

Correspondence
Address correspondence to: Franz Oswald, PhD, Department of Internal Medicine I, Center for Internal Medicine, University Medical Center Ulm, 89081 Ulm, Germany. e-mail: franz.oswald@uni-ulm.de.

Acknowledgments
The authors thank Sabine Schirmer and Roswitha Rittelmann (Ulm) for excellent technical assistance. GSE189756 The RBPJ antibody (7A11) was kindly provided by Prof. Bettina Kempkes, Munich, Germany. Johann Gout is currently affiliated with the Institute for Molecular Oncology and Stem Cell Biology, University Medical Center, 89081 Ulm, Germany.

CRediT Authorship Contributions

Leiling Pan (Formal analysis: Equal; Investigation: Equal; Methodology: Lead; Software: Equal; Validation: Equal; Visualization: Equal; Writing – original draft: Equal)

Medhanie A. Mulaw, Prof. (Data curation: Equal; Formal analysis: Lead; Investigation: Equal; Methodology: Equal; Software: Equal; Validation: Equal; Visualization: Equal; Writing – original draft: Supporting)

Peggy Schwarz, Dr. (Data curation: Supporting; Formal analysis: Supporting; Resources: Supporting; Validation: Supporting)

Bernd Baumann, Dr. (Data curation: Supporting; Formal analysis: Supporting; Methodology: Supporting; Visualization: Supporting; Writing – original draft: Supporting)

Thomas Seufferlein, Prof. (Conceptualization: Supporting; Data curation: Supporting; Funding acquisition: Supporting; Supervision: Supporting)

Martin Wagner, Prof. (Conceptualization: Supporting; Data curation: Supporting; Formal analysis: Supporting; Funding acquisition: Equal; Supervision: Equal)

Johann Gout, Dr. (Data curation: Equal; Investigation: Equal; Methodology: Equal)

Min Guo (Investigation: Equal; Methodology: Equal)

Hina Zarrin (Investigation: Equal; Methodology: Equal)

Franz Oswald, Prof. (Conceptualization: Lead; Data curation: Equal; Formal analysis: Equal; Funding acquisition: Equal; Methodology: Equal; Project administration: Lead; Supervision: Lead; Validation: Equal; Visualization: Equal; Writing – original draft: Equal; Writing – review & editing: Equal)

Conflicts of Interest
The authors disclose no conflicts.

Funding
Leiling Pan is a participating member of the International Graduate School in Molecular Medicine at Ulm University, which is supported by the German Research Foundation (Deutsche Forschungsgemeinschaft) (grant number GSC 270). This work was further supported by the German Research Foundation, (GRK2254/C4 [to Martin Wagner], SFB1074/A3 [to Franz Oswald], SFB1506/A5 [to Franz Oswald], OS 287/4-1 [to Franz Oswald], SFB1506/A5 [to Franz Oswald and Bernd Baumann]) and the German Cancer Aid (Deutsche Krebshilfe) (#70114289 [to Franz Oswald]).